Coastal flood: a composite method for past events characterisation providing insights in past, present and future hazards-joining historical, statistical and modelling approaches

Déborah Idier, Jeremy Rohmer, Rodrigo Pedreros, Sylvestre Le Roy, Jérôme Lambert, Jessie Louisor, Gonéri Le Cozannet, Erwan Le Cornec

Noname manuscript No.
(will be inserted by the editor)

Coastal flood: a composite method for past events characterisation providing insights in past, present and future hazards

Joining historical, statistical and modeling approaches

Déborah Idier · Jérémy Rohmer · Rodrigo Pedreros · Sylvestre Le Roy · Jérome Lambert · Jessie Louisor · Gonéri Le Cozannet · Erwan Le Cornec

Received: date / Accepted: date

Abstract The characterisation of past coastal flood events is crucial for risk prevention. However, it is limited by the partial nature of historical information on flood events and the lack or limited quality of past hydro-meteorological data. In addition coastal flood processes are complex, driven by many hydro-meteorological processes, making mechanisms and probability analysis challenging. Here, we tackle these issues by joining historical, statistical and modelling approaches. We focus on a macrotidal site (Gâvres, France) subject to overtopping and investigate the 1900-2010 period. We build a continuous hydro-meteorological database and a damage event database using archives, newspapers, maps and aerial photographies. Using together these historic information, hindcasts and hydrodynamic models, we identify 9 flood events, among which 5 are significant flood events (4 with high confidence: 1924, 1978, 2001, 2008; 1 with a lower confidence: 1904). These flood events are driven by the combination of sea-level rise, tide, atmospheric surge, offshore wave conditions and local wind. We further analyse the critical conditions leading to flood, including the effect of coastal defences, showing, for instance, that the present coastal defences would not have allowed to face the hydro-meteorological conditions of 09/02/1924, whose bi-variate return periods of exceedance T_R (still water level relative to the mean sea level and significant wave height) is larger than 1000 y. In the coming decades, T_R is expected to significantly decrease with sea-level rise, reaching values smaller than 1 y, for

The BRGM and ANR (RISCOPE project, n° ANR-16-CE04-0011) funding are acknowledged

D. Idier · J. Rohmer · R. Pedreros · J. Lambert · J. Louisor · G. Le Cozannet
BRGM, 3 av. C. Guillemin, 45060 Orléans Cédex, France
Tel.: +33 2 38 64 35 68
E-mail: d.idier@brgm.fr

S. Le Roy
BRGM, 2 Rue de Jouanet, 35700 Rennes, France

E. Le Cornec
GEOS-AEL, 12 Rue Maréchal Foch, 56410 Etel, France

8 of the 9 historical events, for a sea-level rise of 0.63 m, which is equal to the median sea-level rise projected by the 5th Assessment Report of the IPCC in this region for RCP8.5 in 2100.

Keywords overtopping · historical events · sea-level rise · SWASH · joint probabilities · sensitivity analysis

1 Introduction

The characterisation (occurrence, mechanisms, probability) of past coastal flood events is crucial for risk prevention (see e.g. *Dangendorf et al.* 2016). However, it is not a trivial task, especially when considering events that occurred several decades ago. Most of the time, the historical information is very partial, with for instance mention of water invading docks or of damages on a given asset. Even partial, this information remains very useful to improve the quantification of extreme water levels, to better estimate potential flood hazards or to understand the impacts of contemporary climate change (*Zong and Tooley* 2003; *Needham and Keim* 2012; *Breilh et al.* 2014; *Jeffers* 2014; *Bulteau et al.* 2015; *Fortunato et al.* 2017; *Wadey et al.* 2017; *Haigh et al.* 2017; *Hénaff et al.* 2018; *Giloy et al.* 2018; *Hamdi et al.* 2018; *Garnier et al.* 2018). However, historical information on flood events is subject to uncertainties: while there is high confidence that reported flood events really occurred, the absence of report does not necessarily mean that there was no flood. This is especially the case on coastal sites with few or no assets until the last decades, and thus where nobody reported the flood event or had reasons to do so.

One key issue in the characterisation of the driving factors of historical flood events and their probability is the availability of past hydro-meteorological data. Flood often results from the combination of several conditions (e.g. tide, atmospheric surge, waves), so that all these conditions must be characterised for accurate assessment. There are two approaches to estimate these conditions: using measurements or modelling. However, the spatial coverage of measurements is limited, and their temporal coverage ranges from about a century (the longest available tide gauge data, as in Brest, France) to few years only. While modelling requires significant effort, many retrospective simulations (hereafter: hindcasts) have been produced over the last decade and deliver reconstructions of pressures, winds, waves or atmospheric storm surges. Some hindcasts go back to the end of the 19th century (see e.g. 20CR for meteorological hindcasts, from *Compo et al.* 2015), opening the perspective of better characterising events that occurred several decades ago. However, their quality is still lower than the one of hindcasts limited to shorter and recent period (see e.g. CFSR, from *Dee et al.* 2014). As a consequence, the characterisation of the driving factors of such historical event is rarely done and their probability is not estimated.

In practice, when a coastal flood model is validated in a given area, it is most of the time on a single (recent) event (see e.g. *Wadey et al.* 2013; *Bertin et al.* 2014; *Le Roy et al.* 2015), and more rarely on several events (see e.g. *Gallien et al.* 2018, for a discussion on coastal flood modelling challenges). This is even more true for overtopping flood events, which are more difficult to model. In addition, the limited knowledge of past hydro-meteorological conditions challenges our ability

to identify the critical hydro-meteorological conditions, which can led to flood. However, such knowledge is crucial not only for early-warning systems but also to anticipate the potential effect of sea-level rise in the future.

The present paper aims at demonstrating how knowledge of past event occurrence, their driving conditions and probability can be improved by joining historical, statistical and modelling approaches. We focus on a macrotidal site (Gâvres, France) subject to overtopping and investigate the 1900-2010 period. First, the site, method and flood model are described (Section 2). Section 3 describes the databases and the added value of the model simulations to identify past flood events. Section 4 describes the main flood events, identifies hydro-meteorological conditions leading to flood events, estimates their probabilities, analyses the sensitivity of flood event to changing forcing conditions and evolving coastal defences, and investigates the effect of sea-level rise. The method, results, limits, and implications for local risk prevention and early warning systems are discussed (Sect. 5) before drawing the conclusion.

2 Site, methodology and model

2.1 Gâvres

Gâvres is located on the French Atlantic coast (Figure 1a), in a macro-tidal environment (mean spring tidal range: 4.2 m). This site is mainly subject to overtopping, as illustrated for instance by the past flood event of the 10th of March 2008 (*Cariolet* 2011; *André* 2014; *Le Roy et al.* 2015). Its surface area is smaller than 2 km^2. In 2015 there were 695 inhabitants (and 752 in 2009), after the national French statistics (INSEE). This population is multiplied by 5 in summer. During the 2008 flood events, about 120 houses were flooded, after the data provided by the town hall (Figure 1b). As a preliminary analysis of critical water levels (including still water levels and waves) for flood, a bathtub method accounting for the connectivity (see e.g. *Poulter and Halpin* 2008) was applied to a Digital Elevation Model (DEM_{2008}) representative of the 2008 topo-bathymetry (Figure 1a; see section 2.3). We find that land is flooded for nearshore water levels larger than 3.77 m IGN69 (national vertical datum).

Local waves are affected by the presence of an offshore island (Groix) located at the West of the study site (Figure 1c), such that the offshore wave conditions between the site and Groix are strongly non-uniform. This local non-uniformity makes the identification of the wave conditions leading to flood events not straightforward. To tackle this issue, offshore wave conditions need to be considered. Here, after some wave modelling tests (not shown), the local non uniform wave conditions can be satisfactorily modelled by propagating waves observed south of Groix (Figure 1c, grey star).

Since more than 10 years, a lot of knowledge has been gained on the time evolution of the territory of Gâvres, its coastal defences and past flood events. The first key study was performed by *Le Cornec and Schoorens* (2007) as part of a flood hazard assessment for regulatory coastal risk prevention plans. Since 1900, there have been many modifications of the territory. First, about half of the buildings were built after 1950 (Figure 2 ; see also *Le Cornec and Ferrand* 2009; *Le Berre et al.* 2012). Before 1915, there were no coastal defences, except along the

narrow part of the site and the east part of the tombolo (the so-called "polygone" area). However, at that time, there were large coastal dunes. But in the early 1940's (second world war), significant volume of sediment has been extracted from these dunes for construction purposes (*Le Cornec et al.* 2012). After the local authorities, this extraction weakened the capacity of the dunes to protect the land from floods (for further details see *Le Cornec et al.* 2012). The urban development started in the 1950's (most of the area flooded in 2008 was a lagoon in the 1900's), and coastal defences have been progressively built along the coast, to fix the shoreline, with the aim of protecting inland assets from flood and erosion. These coastal defences were damaged and consolidated many times (*Le Cornec and Peeters* 2010). Hence, a recent upgrade of coastal defences was implemented after the 2008 flood event.

In addition to land cover and coastal defences changes, the analysis of aerial photographs shows that rocky outcrops that were not visible in 1932 appear now on recent images in front of the Grande Plage beach, and that the overall surface of visible rock outcrops is increasing with the time (Figure 2; see also *Le Cornec and Peeters* 2010). This suggests a general trend toward a decrease of the intertidal sediment volumes and a lowering of the intertidal topography. Consistently, two groins were built in 2012 just at the east of the study site, along the south beach of the tombolo, in order to prevent erosion and potential subsequent flood. Since then, the beach was nourished several times.

2.2 Method

To investigate the past flood events and the conditions leading to flooding, we follow the method summarised in Figure 3.

The first step consists in collecting all the information available on the study site: in addition to scientific literature, this includes technical reports, coastal hazards studies, local events knowledge, risk management practices, historical evolution of coastal defences and assets, etc. This allows drawing a first overall picture of the main past flood events and factors causing flood. Then, two databases are built: a damage events database (DED) and a hydro-meteorological database (HMD). DED contains damage events resulting either from flood or from other drivers (wind, erosion, etc.), and, for each event, a flood occurrence indicator and its confidence indicator. The hydro-meteorological database contains continuous time series, at least for water levels (including sea-level rise, tide and atmospheric storm surge) and wave conditions. Locally the wind can also be a key driver, so that the local wind conditions needs also to be estimated over the study period (here, this is case, as it will be shown in the present paper).

Then, a preliminary comparison of DED and HMD is performed, in order to identify if there are extreme hydro-meteorological conditions corresponding to no flood events. If this happens, then further research of historical archives describing the damages is required to reduce the uncertainties on these suspicious events. This analysis potentially allows improving the quality of the DED database. A numerical model relevant for the study site can be used optionally (this is the case in the present study) to comfort the quality of the damage events database and to help guiding the historical information survey. First, the model is used to compute the flood or flood occurrence indicator (e.g. water volume invading the land) related to the events of the DED database. This step leads to the creation

of a coastal flood model database (CFD). Then, the DED and CFD databases can be compared to refine the confidence in the identified flood events of the DED database, and to identify potential events for which both databases disagree. If the model results suggest a significant flood whereas historical information is uncertain, or if the event is known as a "no flood" event, then further research on historical information (archives) is pursued. If additional historical information is found, the DED database is updated.

After this loop, we assume that the DED database is the best that could be achieved. Then a deeper analysis of the datasets is performed, for instance by characterising the critical hydro-meteorological conditions leading to flood, estimating their probability of exceedance and the potential changes with sea-level rise. In the present study, the model is also used to better understand the flood occurrence sensitivity to the hydro-meteorological forcing parameters.

2.3 The coastal flood modelling: models, set up, and flood indicator

To support the flood event analysis, a numerical model is set up with the objective to provide indicator of flood events (in terms of occurrence and even in terms of relative intensity), with a good accuracy, but with an affordable computation time.

To ensure the accuracy, we use the non-hydrostatic phase-resolving model SWASH (*Zijlema et al.* 2011), which allows simulating wave overtopping and wave overflow. The computational domain is shown in Figure 1a. The space and time resolution are respectively 3 m and more than 10 Hz. The topography and bathymetry are based on bathymetric surveys (SHOM, DHI), lidar (public RGE-Alti®1m product) and GPS survey on coastal defences. In addition we propagate the offshore wave conditions (south of Groix) to the boundaries of the SWASH model using the spectral wave model WW3 (*Ardhuin et al.* 2010), taking into account the local wind (computation domain shown in Figure 1c). To summarize: WW3 propagates the offshore wave conditions, taking into account the local wind and still water level; wave parameters (H_s,T_p,D_p) are extracted along the boundaries of the SWASH computational domain; SWASH is run with the non-uniform wave boundary conditions, the still water level and the local wind.

This model chain has been validated in terms of flooded area on the 10/03/2008 flood event (called Johanna) (see *Le Roy et al.* 2015, for more details on the flood event). The Digital Elevation Model (called DEM_{2008}) used as input of SWASH is representative of this Johanna event (see *Le Roy et al.* 2015). For this validation, the model has been run for an event that lasts over 6 hours, centred on the high tide (i.e., starting 3 h before high tide and ending 3 h after), using the best available forcing conditions: still water level modelled in (*Le Roy et al.* 2015), wave and wind extracted from the HMD database (see section 3.1). Figure 1b shows that there is a reasonable agreement between the modelled maximal high water during the event and the observed flood extension (flooded houses).

One key issue for the simulation of past flood events is the availability of topo-bathymetric data that prevailed at that time. Here, there is no precise topographic data covering the entire study area and the study period prior to the LiDAR data's (i.e., here, prior to 2008). Thus, we cannot rigorously reproduce the actual flood extension of past events, but we can investigate flood event occurrence by focusing on water volume entering inland, keeping in mind the uncertainty related

to temporal changes of the topo-bathymetry. Modelling events that last 6 hours is time consuming (60 hours on 48 cores). Thus, to provide flood indicators, but with a reduced computation time, we focus on the water volume entering inland (Vol) at high tide, over a 15 minutes time lapse. We estimate this water volume by running the WW3 model first (over 2h to reach steady wave conditions), and then the SWASH model over a 20 minutes window. Such simulation costs 1h30min of time computation on 48 cores approximately. Considering that the spin-up of the SWASH simulations can take a few minutes (but is always smaller than 5 min), the flood indicator (Vol) is computed by estimating the inland water volume at the time steps t=5 and t=20 min, and then computing the difference. Atmospheric surge, wave and wind conditions exhibit small changes at hourly time scales (this has been checked also on the HMD data), so that the selected indicator is representative of the flood event intensity, and thus can be used to rank the flood events according to their severity.

3 The databases

3.1 The hydro-meteorological database (HMD)

The HMD database includes reconstructed time series of the hydro-meteorological parameters, which can potentially control the flood on Gâvres, from 1900 to 2010.

Based on the preliminary site analysis and modelling tests, we identify that the following hydro-meteorological factors are those affecting coastal flood: the still water level (mean sea-level, tide and atmospheric storm surge), the wave conditions (height, period, direction) and the local wind conditions (speed and direction). In addition, preliminary modelling tests allow defining relevant geographical locations of extraction for each of these parameters. The still water level is estimated close to the site (black star in Figure 4b). Wave characteristics South of Groix are shown representative of offshore wave conditions (grey star in Figure 4b; see section 2.1), the modelling allowing to propagate these offshore conditions to Gâvres. Finally, the local wind between Groix and Gâvres (black box in Figure 4b) is needed.

There is no tide gauge measurement close enough to the site and covering the entire study period to estimate still water levels (ξ): for example, the tide gauge located in Port Tudy (located approximately 10 km away from the study site) has records back to 1975 only. Thus, we reconstruct each component of ξ (mean sea level, tide, atmospheric storm surge) over the 1900-2010 period, such that ξ is the sum of the 3 components. This approach implicitly assumes that there is no interaction between sea-level rise, tide and surge, an assumption which is justified on this site after the studies of *Idier et al.* (2012, 2017).

For the mean sea level (relative to the land), we first reconstruct mean sea level changes following the procedure of *Rohmer and Le Cozannet* (2019) (see Appendix A). Then, we reference the sea level time series to the vertical datum IGN69, based on the vertical reference data provided in (*SHOM* 2014). To transform these absolute values to values relative to the ground, the data is corrected from the vertical land movement using the 3 nearest GPS stations data provided by the SONEL network (*Santamaría-Gómez et al.* 2017). As shown in Appendix A, the vertical land motion trend at these 3 stations is negative (subsidence). The mean (computed with the least mean square method) provides a vertical land

movement of -0.33 ± 0.15 mm/y. The final relative mean sea level time series (MSL) at Gâvres is plotted in Figure 5.

We use the tidal component database FES2014 (1/16° resolution ; *Carrere et al.* 2016) to reconstruct the tide. To assess the FES2014 quality, we compare predictions at Port-Tudy (Groix) with the tide gauge based tidal predictions (SHOMAR). The correlation coefficient (r) is equal to 0.999.

For the atmospheric storm surge, waves and wind, we rely on hindcasts. Several datasets are available, but none of them covers the entire period with a sufficient quality. Thus we combine datasets of different qualities and reduce bias between them by using a non-parametric quantile mapping using empirical quantiles (referred to as quantile-quantile (QQ) method in the following; see e.g. *Gudmundsson et al.* 2012, for a review on the methods). These biases can be due to either the intrinsic quality of the dataset, or an insufficient spatial resolution (such that the point at which the data are extracted is different from the relevant location of extraction). Table 1 contains the sources of each datasets. Figure 4a illustrates the periods covered by each dataset and the method we used to set up continuous time series over the study period.

For the storm surges, we selected three datasets. For the most recent period, we use the 250 m resolution MARC hindcast (2006-2016), whose quality has been proven (see e.g. *Muller et al.* 2014). The two other datasets are based on atmospheric pressure hindcasts (CFSR, 20CR), from which the surge is estimated using the inverse barometer (IB) approach. Because such estimated surge does not account for the wind induced storm surge, the resulting estimate is not expected to be accurate. However, using the QQ correction of these datasets allows to indirectly account for this wind-induced surge (as the MARC hindcast accounts for the pressure and wind induced storm surge). The CFSR-IB dataset is corrected with the QQ method using the MARC dataset on the overlapping period. Then, a QQ correction is done on the 20CR-IB dataset relying on the corrected CFSR-IB dataset. In both cases (see Figure 15a,b in Appendix B), this leads to an increase of the under-estimated surge values of about 0.10 m for the largest surge values (above quantile level of 99.9%, i.e. above ~ 0.50 m). It should be noted that due to the resolution of 20CR, the extraction point is far from the location of interest (200 km, Figure 4c), but the QQ correction contributes to indirectly propagate this surge to the location of interest. At the end, we concatenate the datasets, such that on overlapping periods, the best quality dataset is always selected. Figure 4a shows the period for which we extract each dataset.

For the waves, the highest resolution hindcast available on the study area are Homere and Norgasug (*Boudiere et al.* 2013). These hindcasts have a spatial resolution of a few hundred meters close to the coast. A comparison of the dataset with measurements (on overlapping dates) is done at the closest wave buoy (Candhis network, buoy n°05602 located further South, 47°17.1'N, 3°17.1'W). Norgasug provides the best correlation coefficients (r=0.98, 0.79, 0.61, for H_s, T_p, D_p, respectively), so that it is selected in priority. Then, the dataset is built backward as follows: Homere, BoBWA (10 km resolution), Sonel-waves (based on 20CR wind forcing). As for the surges, we apply QQ corrections to improve the quality of the wave data. First, we correct the local Homere data using the Norgasug hindcast over the 2008-2016 period. As highlighted by Figure 16a,b,c in Appendix B, the distributions (before correction) are quite close. The QQ correction leads to H_s changes smaller than 0.50m for the highest waves (above the 99.9% quantile level,

i.e. above 6.20 m), T_p changes of about 1s for T_p values above 16 s, and a clockwise correction of a few degrees for the main mode (with a shift from 262°N to 265°N).

Then, Bobwa and Sonel-waves are corrected using the corrected Homere hindcast, as they do not overlap the Norgasug hindcast. The resulting correction of Bobwa (Figure 16d,e,f in Appendix B) compares well with the one of Homere (Figure 16a,b,c) with a small decrease of H_s ($\sim$ 0.40 to 0.50 m) for the highest waves (H_s larger than the 99.9% quantile level of $\sim$ 7 m), a slight decrease (in average) in T_p and a few degrees of counter-clockwise correction in D_p for the main mode (with a shift from 267°N to 265°N). The corrections of the Sonel data are much larger (see Figure 16g,h,i), which is expected because the Sonel wave extraction point is located much more offshore (Figure 4b).

Regarding the wind, we first use the CFSR (1979-2010) hindcast to provide wind speed and directions for the most recent period. To complete the time series, we use the 20CR hindcast and correct it with the QQ correction method, using the CFSR data (Figure 17 in Appendix B). This leads to decreasing the 20CR wind speed of up to almost 7 m/s for quantile levels above 99.9% (i.e. $U > 20$ m/s), and to a clockwise rotation of about 15° for the main mode (with a shift from 245°N to 260°N), which is also the one corresponding to the largest wind speeds.

Finally, the HMD database covers the 1900-2010 period with a 10 min time step (linear interpolation). Figure 5 shows the distribution of each hydro-meteorological variable. The maximum values of the relative mean sea level, tide, surge, significant wave height, wave peak period and wind velocity are 0.52 m IGN69, 2.63 m, 0.83 m, 9.18 m, 25.20 s and 27.67 m/s respectively. The dominant wave direction is 265°N (i.e. from W-SW), while the wind direction is bimodal with a dominant mode at 260°N.

3.2 The historical damage events database (DED)

3.2.1 Initial set up

To set up the damage event database, we start from the study of *Le Cornec et al.* (2012), which referenced 44 damage events between 1900 and 2010 based on the Gâvres municipal archives, State Department archives (Bridges and Highways, Maritime Services), military archives and newspaper articles. This first dataset was completed with further research revisiting newspapers dated back up to 1900 (*Lambert* 2017), which led to identify 4 additional damage events (13-15/02/1900; 7-9/12/1911; 11/04/1922; 13-14/03/1937), and provided complementary information on 4 events (02/02/1904; 09/01/1924; 26-27/11/1924; 27/01/1936). This additional information also includes some reports on storm impacts in Port-Louis and Lorient (close to Gâvres). Then we classify each event in terms of flood event (F): 0 (no flood), 1 (moderate flood; e.g. few waves overtopping coastal defences), 2 (massive flood). In addition, we assess the uncertainty (C) of this classification (1: medium confidence, 2: high confidence). As a general rule, for every certain flood event, a confidence indicator of 2 is given. For all the other events, a confidence value of 1 is used in the first version of the database, before critical review with respect to numerical and statistical modelling. Indeed, the historical information available on these medium confidence events concerns mainly shipwrecks or coastal defence damages (erosion), and inland damages, but which seem related

to the direct effect of wind, rather than flood. For all these events, there is no information on potential flood or waves overtopping the defences. However, this does not guarantee that no waves overtopped the defences at that time. The list, dates and classification of the identified events are given in Appendix C (Table 5, $F1$ and $C1$ indicators). Some events, especially the oldest ones, are not always well identified in time (in Appendix C, see e.g. the event Nd=6 which is referenced between the 12 and 20^{th} of October 1922), while the damage event is identified with an half-day resolution on the last decades.

The DED database includes 48 damage events between 1900 and 2010. Among them, 9 correspond to a flood event. Among these flood events, 5 seem to be characterised by moderate overtopping or moderate flood (02/02/1904, 07/02/2001, 27/10/2004, 10/02/2009, 28/02/2010), while the 4 others definitively correspond to significant flood events (09/01/1924, 26/02/1978, 10/01/2001, 08/03/2008). Especially for the first half of the XX^{th} century, the absence of information indicating a flood does not mean that there was no flood. Indeed, the urbanisation has strongly increased after 1950 (most of the areas flooded during the Johanna event (2008) were not built in 1950, see Figure 2). This implies that moderate flood events have not necessarily been observed, and this could explain why the moderate overtopping events have been mainly identified over the last decades. Thus, the 9 flood events should be considered as a low bound of what really happened between 1900 and 2010. This is an inherent limitation of any historical database. Regarding the 1904 damage event, there was no clear indication of local flood. However, one of the available archive (SHM1 in Table 1) stated that "lors du raz de marée ... les parapets de sable sans soutien intérieur ont été absolument impressionnant à arrêter l'invasion de l'eau" (translation: *During the tidal wave ... the parapets of sand without inner support were absolutely impressive in stopping the invasion of the water*), suggesting that a massive flood event ("raz de marée") occurred at least in the surrounding, but that the land behind the parapets (here, the tombolo at the east of the study area) were not flooded. Based on this information, we cannot ensure there was no flooding anywhere on the Gâvres land. In addition, at Lorient (city located at about 5 km at the North of Gâvres) the 1904 event was considered at that time as a storm which would remain in memories as one of the most damaging event in the region (see the article entitled "Un raz de marée" from the "Courrier des Campagnes" journal of the 7^{th} of February 1904). Thus, we classify the 1904 event as a moderate flood with a medium confidence index. Following our approach (Figure 3), this first version is refined in the next paragraph.

3.2.2 Validation, modelling contribution and update

For each damage event of the database, we extract the hydro-meteorological conditions at high tide (see Appendix C). When extreme hydro-meteorological conditions are identified in the HMD but can not be associated to any flood event in the DED, we seek clues in new complementary historical information, and eventually use them to re-evaluate the flood and confidence indicators. In our case, the model presented in section 2 can be used to identify such events. To do so, we compute the flood indicator (Vol) on each hydro-meteorological conditions associated to the damage events, for the DEM_{2008}, keeping in mind that the coastal defences and the nearshore bathymetry (upper part of the beach) changed significantly over

the time, so that the model results should be used as an indicator, rather than an accurate reconstruction of what actually happened during the event. Then:

- For damage events such that $F = 0$ and $C = 1$, if $Vol > 0$, then we keep the initial value of F and C; else if $Vol = 0$, the model results and partial historical knowledge agree such that the confidence is increased and C is equal to 2.
- For damage events such that $F = 1$ and $C = 1$, if $Vol > 0$ and additional historical information indicates a significant flood, then $F = 2$ and either $C = 2$ (if the historical information are precise and local) or $C = 1$.

First, for 17 of the 39 "no flood" events of the initial version ($F1 = 0$) of the database, the model predicts that no flood occurs ($Vol = 0$). Thus, the confidence is increased to $C = 2$ for these 17 events. Second, the model predicts the 9 flood events ($F1 > 0$) identified in the initial version of the DED database (Figure 6). This reinforces the confidence in the model skills. However, ranking events according to their intensity using the modelling results and the DED leads to different results for the events of 1904, 2001, 2009 and 2010.

The largest volume is obtained for the 1904 event, suggesting that a massive flood occurred at that time. Thus, further newspaper research has been pursued. We found one reference (*Le Matin*, 05/02/1904, see Table 2) stating that "Mais sur toute la côte, à [...] Gâvres [...], tous ces petits ports où la mer bat au pied des maisons, furent balayés en partie par les lames qui arrachaient des maisons" (translation: *But all along the coast, at [...] Gâvres [...], all these small harbours where the sea beats at the foot of the houses were swept by the sea which tear off the houses*). The 1904 event is one of the events characterised by the largest still water level, wave height, wave period and wind (it can be seen by comparing the 1904 values of Table 3 with the distribution of the HMD database shown in Figure 5). In addition, in 1904, all the area flooded during the Johanna event was uninhabited and still connected to the sea (Figure 2). This could explain why this event did not appear as a drastic flood in the contemporary newspapers. However, the topo-bathymetry probably changed significantly between 1904 and 2008 (there were large dunes and probably a higher intertidal beach, see section 2). In addition, if a massive flood really occurred in Gâvres in 1904, it is still a bit surprising to find so few proofs of floods, in particular considering the significant amount of information found for the older flood events on the Gâvres tombolo (e.g. in 1866 or 1896) or for the same 1904 events but on the surrounding towns (*Le Cornec et al.* 2012). Based on these elements, the DED database is updated for the 1904 event by setting $F2 = 2$ (massive flood) but with $C2 = 1$ (medium confidence), as there are still doubts on the massive character of this historical flood event in Gâvres.

During the January 2001 event, coastal defences fully collapsed along the southern beach. Because our digital elevation model (DEM_{2008}) does not account for this collapse, we obtain a low flood indicator value using the model. After the 2008 flood event, the coastal defences were raised. To account for this upgrade of coastal defences, we set up a second DEM ($\mathrm{DEM}_{upgrade}$) based on the DEM_{2008} but including higher coastal defences. Specifically, we use GPS and theodolite surveys to determine the new coastal defence height. These surveys were performed in 2017, but still reflect the current status of coastal defences as they were not upgraded after the beginning of 2009. Taking into account this upgrade leads to $Vol = 0$ and ~ 35 m^3 for the 2009 and 2010 events respectively. This is consistent

with observations, as few overtopping were reported in 2009 and 2010. In addition, these values are much smaller than for the 1904, 1924, 1978 and 2008 events (considering the DEM_{2008} for these 4 events). This hierarchy in the intensity of flood events is consistent with the DED database.

The cross-fertilization of historical information and the model results leads to changing 18 events in the damage database, mainly their confidence indicator (17 events over 18). Appendix C includes the final version of the database ($F2$,$C2$), and Table 2 provides the newspapers and archives considered for the 9 flood events.

4 Analysis

4.1 Flood events characteristics

Significant and moderate (overtopping) flood events are indicated in Table 3, together with their hydro-meteorological conditions.

Figure 7 shows the storm tracks of these 9 flood events. They exhibit very different patterns, with for instance the 2010 storm coming from SW and the 2008 storm coming from NW (Greenland). The travel speeds of these storms also display significant differences, with the 1904 storm being the slowest one (see how close the dark blue dots are in the Celtic Sea and English Channel), meaning that this storm affected the surrounding of Gâvres during a long time. The 2001 event includes two storm tracks, while the 2010 storm moved very quickly.

In the present study, we consider the 8 following forcing conditions: mean sea level, tide, surge, wave height, wave period, wave direction, wind intensity and wind direction. This 8 dimension problem can be reduced to a 6 dimension problem by replacing the three first components by the resulting still water level ξ. Figure 8 shows all the damage events in this 6 dimension hydro-meteorological domain. The 5 main flood events correspond to different settings. The 1924 and 1978 events are characterised by high still water level (3.14 and 3.06 m IGN69), high ($H_s = 8.5$ and 5.6 m) and long waves ($T_p = 21.2$ and 18.8 s), and moderate winds ($U = 7.2$ and 10.5 m/s) from NW and SW. The 2001 flood event is characterised by a lower still water level of 2.97 m IGN69, smaller ($H_s = 3.5$ m) and shorter waves ($T_p = 11.2$ s), and stronger winds (13.5 m/s) from SW, but we should keep in mind the 2001 collapse of coastal defences along the South beach (Grande Plage). The 2008 flood event is characterised by a much larger still water level of 3.42 m IGN69, large wave height ($H_s = 5.53$ m) and moderate period ($T_p = 11$ s), for even stronger winds (18.2 m/s) coming from W. The characteristics of the 1904 event look similar to the 2008 event (large water level, large wave height) but with a larger wave period ($T_p = 15.1$ s). Finally, the damage event associated with the highest still water level ($\xi = 3.47$ m IGN69) corresponds to the 2010 Xynthia storm, but this event is identified as a moderate flood event, since overtopping only was observed. The corresponding hydro-meteorological conditions are quite similar to the one of the 2008 flood event, but with a significant wave height twice as small. This suggests (and is confirmed by the model simulation) that without coastal defences upgrade early 2009, the Xynthia storm would have led to a much larger flood event.

After the testimonies (*Le Cornec et al.* 2012), the recent flood events (February 2001, 2004, 2008, 2009, 2010) were induced by wave overtopping. After the model results, the flood is mainly induced by wave overtopping for the 9 flood events,

whatever the DEM considered (DEM_{2008}, $DEM_{upgrade}$). This suggests that the main flood regime since 110 years is overtopping.

4.2 Critical hydro-meteorological forcing conditions

4.2.1 Based on databases

The cross-analysis of the Hydro-Meteorological and Damage Events Databases provides indications on the critical forcing conditions leading to flood (Figure 8). First, the minimal still water level above which flood occurred is estimated to be $\xi_c = 2.77$ m IGN69. Second, from the scatter plot (ξ, H_s) we can draw a critical contour above which all the flood events occurred (red dotted line). The minimal peak period above which all significant flood occurred is $T_{pc} \sim 11$ s (scatter (ξ, T_p)). The minimal wind speed above which all significant flood occurred is $U_c \sim 7$ m/s (scatter plot (ξ, U) in Figure 8). This analysis suggests that the main drivers are the still water level and wave height, the effect of these drivers being modulated by the wave period and wind velocity.

In the above analysis we considered the still water level ξ, which includes the mean sea level, tide, and surge. Figure 9 shows the contribution of each of these three water level components. Comparing the first (1904) and last event (2010, corresponding to the largest still water level), we find that mean sea-level rise ($\sim$ 21 cm) contributes to 87% of the difference in ξ (24 cm). This difference in mean sea levels is comparable to the variability of the surges associated to the flood events. This highlights that past sea-level rise has already significantly altered the hydrodynamic forcing in Gâvres. Such increasing effect is not directly visible in the simulated floods over the 1900-2010 period (Figure 6), as flood is driven not only by the still water level, but also by the waves. However, we could wonder how a flood induced by the 1904 forcing conditions would look like for the present mean sea-level (see section 4.4).

4.2.2 Based on numerical simulations

The damage database contains "only" 48 events. Characterising the flood sensitivity to the 6 hydro-meteorological components based on information on 48 events only is challenging. In addition, as discussed above, the topo-bathymetry has evolved over time. Thus, to further explore the flood sensitivity to the forcing conditions, we use the model simulations, considering a fixed topo-bathymetry (here, the DEM_{2008} configuration). In addition to the 48 simulated historical events (section 3.2.2) we made many other simulations (300) that we use here to identify the critical hydro-meteorological conditions leading to flooding. This represents 348 simulations, which are distributed as follows: : (i) 78 corresponding to the hydro-meteorological conditions listed in Figure 14, (ii) 90 corresponding to a sensitivity study to the wind direction for the hydro-meteorological conditions associated to the 1904, 1924, 1978, 2008 and 2010 flood events ; 20 corresponding to the historical conditions of the HMD database characterised by the largest still water levels (but not corresponding to events of the Damage Event Database), (iv) 160 focusing on the Johanna event and varying each parameter, keeping the others fixed. However, this dataset explores conditions around those related to

events listed in the damage database. To complete this dataset in a larger domain, we set up 100 additional scenarios. For this purpose, we followed the methodology described by *Gouldby et al.* (2014) to select a limited number of extreme, but realistic, forcing conditions to be used as inputs of the simulation model. This task was conducted by combining two methods. First, a multivariate extreme value analysis was conducted to randomly generate via a Monte-Carlo procedure a large number of offshore conditions (here chosen as 150,000 realizations), namely ξ, H_s, T_p, D_p, U, D_u, by taking into account extreme values (and their dependence structure) based on the method described in Appendix D (but applied to events with high tide amplitude larger than 2.342 m and surge peak larger than 0 m). Second, 100 scenarios are selected from this dataset by means of a clustering algorithm based on maximum dissimilarity (MDA algorithm *Willett* 1999), and 100 additional simulations are done.

We analyse the results of these 448 simulations in each of the bivariate input space (Figure 10) as follows. The bivariate space is discretized in regular cells. Then, in each cell, we compute the ratio r between the number of simulations leading to $Vol > 0$ and the total number of simulations done in this cell. First, critical contours can be identified in the (ξ, H_s) and (ξ, T_p) spaces, as in the analysis of the hydro-meteorological conditions related to the damage event database. For D_p, a critical contour below which flood is favoured can also be seen. This critical contour is such that D_p increases with ξ. Regarding the wind speed, r is increasing with increasing U, and for $U > 20$ m/s, all the simulations lead to flood event. Regarding the effect of Du, the pattern is less clear, but it seems there is a range of direction (from about 90 to 240 °) favouring flood events.

To better assess the sensitivity to the wind direction, we investigate the effect of Du for the three past flood events subject to the largest local wind speed (Figure 8), i.e. the 1904, 2008 and 2010 events, with Du ranging between 0 to 340°, and $\Delta Du = 20°$. Figure 11 shows that whatever the wind direction, Vol is always larger than 0, such that the flood occurrence is not sensitive to Du for these events, contrary to the Vol intensity which is very sensitive to the wind direction, reaching its maximum for $Du \sim 230 - 240°$. For the 1904, 2008 and 2010 events, the volume is increased by 17%, 256 %, and 466 % respectively, between its minimum and maximum values $((\max(Vol) - \min(Vol))/\min(Vol))$. On such a small domain (about 10 km between the offshore wave conditions and the study site), a so significant effect of local wind direction was not expected. The fact that wind direction of 230-240° are favouring flood can be physically interpreted as follows: the wind not only generates local waves, but also modifies the swells, in such a way that deep water swells coming from a given direction D_p are amplified by winds coming from a similar direction ($D_p \pm 30°$), after *Aarnes and Krogstad* (2001). At the scale of the computational domain, the analysis of the spectral wave model (WW3) outcomes (see the black contour on Figure 1c) shows indeed that the largest regional scale wave height is obtained for simulations with a wind direction close to the wave direction. This explains the bump observed on the curves. The bumps are not exactly centred on the wave direction (248, 256 and 190 ° respectively) because of the local nearshore wave refraction. As an illustration, Figure 12 shows the regional wave propagation for the hydro-meteorological conditions corresponding to the Johanna event (panel b) and how the wave pattern changes with the direction of the wind acting on the computational domain (panel a): (i) winds coming from 240° leads to the largest waves at the regional scale (panel a),

(ii) at the more local scale, H_s (extracted at the location indicated by the black dot on panel b) is also maximum for the 240° wind direction (panel a, polar plot) with $H_s = 2.9$ m to compare to $H_s = 2.3$ m for northern winds. Thus, local winds from SW direction appear as the most dangerous in terms of flood occurrence. Figure 11 also shows that the wind direction of the 2008 and 2010 flood events (black diamonds) falls outside the most unfavourable range, while the direction corresponding to the 1904 event corresponds to the most adverse direction.

The above critical conditions have been obtained considering a given topo-bathymetry and coastal defence scheme (DEM_{2008}). However, as suggested in section 3.2.2, coastal defences play a significant role on the flood intensity. For instance, the Vol indicator is divided by 8 for the Johanna event with the upgraded coastal defences compared to its reference value obtained for the 2008 coastal defence scheme (Figure 6). However, Vol is still not null, so that (moderate) flood is still expected even with upgraded coastal defences. For the 2009 and 2010 events, our results show that the coastal defence upgrade significantly reduced the flood. Thus, the critical hydro-meteorological conditions identified above should be considered as a secure estimation, as they assume lower coastal defences than those currently in place.

4.3 Hydro-meteorological conditions and flood events: occurrence probability

Over 110 years, at least 4 significant flood events occurred. This suggests an empirical return period of significant flood on Gâvres area of about 25 years. However, due to the uncertain significant flood event of 1904, there could have been a maximum of 5 significant flood events, such that 20 years could be considered as a low bound for the return period of significant flood events, keeping in mind that this is only an empirical estimation, which should be considered with caution. However, the topography and coastal defences have strongly evolved over the century and these 10 last years after the Johanna event, which led to increase the coastal defence height. In addition, no reliable estimate of the return period of floods (whether significant or not) can be provided using the present database, as events with moderate overtopping have probably not been reported during the first half of the century (see section 3.2).

However, using the continuous HMD database which covers 116 years (Figure 4), we can characterise the probability of occurrence of offshore conditions that led, in the past, to significant or moderate flood. For this purpose, bivariate extreme value analysis (bEVA) is performed by focusing on the still water level relative to the mean sea-level ($\xi_{/MSL} = \xi - MSL$) and wave height (H_s), which appeared as the main drivers (see section 4.2.1). The objective of bEVA is to extrapolate the joint probability density of the offshore sea condition variables to extreme values with appropriate consideration of the dependence structure. Using the HMD database, we follow a similar procedure as the one described by *Nicolae-Lerma et al.* (2018). The details on the procedure and application to our datasets are provided in Appendix D. Figure 13 shows the return periods of exceedance (T_R) obtained with this method. Amongst the 5 significant flood events, the offshore conditions ($\xi_{/MSL}; H_s$) of the significant flood of the 10^{th} of January 2001 have the smallest return period of exceedance. This suggests a significant role of the coastal defence failure that took place during this event. The 1924 event offshore

conditions exhibit the largest return period (> 1,000 y), while $T_R \in [100 - 200]$ y and $T_R \sim 100$ y for the 1904 and 2008 events conditions, respectively. We can also notice that the 2010 event offshore conditions had a return period ($T_R \sim 20$ y) larger than the one of 1978 ($T_R \sim 10$ y).

4.4 Impact of sea-level rise

As highlighted in section 4.2.1 and in a number of other locations (*Haigh et al.* 2011; *Hallegatte et al.* 2013; *Arns et al.* 2015; *Le Cozannet et al.* 2015; *Haigh et al.* 2016), past and future sea-level rise (SLR) should significantly alter flooding. In the previous paragraph, the joint return period of water level and wave height was estimated considering the reconstructed mean sea level (Figure 13). This result allows discussing the impact of sea-level rise on return periods. For instance, assuming that the water level ξ_{1904} of the 1904 flood event is reached in 2017, the corresponding tide and surge contribution ($\xi_{/MSL}$) would be smaller, and the return return period of exceedance T_R would be decreased by a factor larger than 5 (for the 1904 event: $\xi_{/MSL_{2017}} = 20$ y, to be compared to 100 y $< \xi_{/MSL_{1904}} < 200$ y ; see e.g. the black bar and point of the 1904 event in Figure 13). This analysis is extended to a large range of sea-level rise values (-0.4 to 1 m) and to the 9 flood events. Figure 14 shows the variations of T_R with SLR for each event conditions (as a reference, SLR=0 corresponds to the 2017 year). First, for all events except that of 1924, T_R decreases to values smaller than 1 year for SLR $\leq$ 0.63 m. Such SLR value is equal to the median regional mean sea-level rise at the 2100 horizon provided by the 5^{th} assessment report of the IPCC for the RCP8.5 scenario (data provided by the Integrated Climate Data Center of the Hambourg University, available online: http://icdc.cen.uni-hamburg.de/daten/ocean/ar5-slr.html; *Church et al.* 2013; *Carson et al.* 2016). This suggests that by 2100, the joint conditions (ξ, H_s) corresponding to the past flood events would statistically occur at least once a year.

5 Discussion

5.1 Limitations and perspectives

The present work contains residual uncertainties. First, the damage event database probably lacks small events in the first half century (among the "no flood" events, there could be some moderate flooding events, but which were not reported at that time). For the simulations on past events, we considered the 2008 bathymetry. However, topographic changes are also expected to take place in intertidal area. In particular, we noticed in section 2.1 that, at least between 1932 and 2008, the intertidal beach was lowered by more than 1 m in about 75 y (see Figure 2). In addition, we considered 2 coastal defences configurations only (2008 and an upgraded version representative of the configuration since 2009), although we know that there were massive dunes along the coast one century ago. For these old configurations (coastal defences and bathymetry), the lack of topo-bathymetric data accounts i.a. for the limited confidence in the 1904 event. Regarding the hydro-meteorological database, we used a quantile-quantile correction method to

build consistent long enough time series of hydro-meteorological conditions. Even with this correction, the accuracy of the obtained forcing data is expected to decrease backwards in time. Due to the lack of local measurements, it was not possible to estimate the quality of the database for old events as for instance those of February 1904 and January 1924. Despite these uncertainties, the occurrence and severity of flood events as obtained from the HMD, DED and simulations still agree relatively well. This suggests that the databases and modelling experiments are of sufficient quality to investigate past flood conditions. At least, they allow to identify past hydro-meteorological events which could lead to massive flood under the present-day topo-bathymetry.

Based on this conclusion, we could consider several implications of this work, for instance in terms of extreme value analysis. First, at a regional scale, coastal flood hazard assessment relies on extreme value analysis of offshore hydrodynamic conditions to define scenarios for flood modelling. One key issue when performing extreme value analysis is the availability of long enough data to estimate the return period of interest (*Bulteau et al.* 2015; *Wahl et al.* 2017). A first approach to tackle this issue is to perform a hindcast (*Muis et al.* 2016). This approach requires a significant computational effort. In addition, the quality of meteorological reanalyses is better for the last decades than in the early XX^{th} century, so that high quality hindcast can be obtained only for the last decades. As a consequence, extreme value analysis are rarely done on more than 50 years of data. Then, because our approach based on standard statistical methods and existing hindcasts allows building hydro-meteorological time series over more than 100 years, it appears as an alternative solution when high-quality hindcast cannot be generated on a long enough period (for the return period's estimation). Second, at a more local scale, specific statistical method to account for partial historical information of extreme coastal water levels have been developed (*Bulteau et al.* 2015; *Hamdi et al.* 2018). These methods combine tide gauge measurements and historical information. They are only applicable when historical information can be related to a vertical landmark. This is rare in practice, so that this method has not been used extensively so far. In addition, tide gauge water level observations include the relative sea-level rise, tides, atmospheric surges, but can also include the wave setup. In the present work, we rebuild a 1900-2100 relative mean sea-level, tide and atmospheric storm surge, such that standard extreme value methods can be used.

In future work, it would be interesting to evaluate how tide gauge measurements, corrected hindcasts (back to 1900, following our method), and partial historical information (older than 1900) could be used together to provide extreme value either of the still water level or of the storm tide level (i.e., including still water and wave setup). In addition, it would be interesting to explore other corrections methods (see *Gudmundsson et al.* 2012).

5.2 Local risk prevention and early-warning system implications

Assuming no coastal defence failure (and a fixed topo-bathymetry), the joint probability analysis (Figure 13) highlights that the conditions leading to the largest modelled flood (1904) are not necessary the ones of largest joint return period of exceedance: $T_R \in [100 - 200]$ y for the 1904 event, while $T_R > 1000$ y for the 1924

event. First, it should be kept in mind that we focused on the joint probability of the two main driving variables to determine return periods. However, other parameters like the wave period or local wind also influence the flood. Second, as illustrated in (*Garrity et al.* 2007; *Idier et al.* 2013; *Sanuy et al.* 2019), as long as forcing conditions have a dimension D larger than 1, offshore conditions of return period T_{R1} induce water level at the coast (or flood) whose return period is not equal to T_{R1}. This highlights that the probability of flood, which is the relevant metrics for coastal risk management, can differ significantly from the probability of flood scenarios identified on T_R isocontours. Where $D > 1$, the probability of exceedance of a water level at the coast (or a given flood intensity), called Zc, requires identifying all the combinations of forcing conditions leading to exceed Zc, i.e. locating the critical contour or frontier $Z = Zc$ in the input space. It is noticeable that the black contour of Figure 8 (scatter plot (H_s;ξ)) exhibits a similar shape to the critical contour of water level at the coast obtained by (*Idier et al.* 2013) in a simpler case ($D = 2$).

The knowledge of critical contour or threshold values of hydro-meteorological conditions for flood occurrence is a key information for flood prevention, adaptation and early-warning system. Flood risk management and prevention practitioners in Gâvres already know reasonably well which conditions favour flood. In addition to the regulatory risk prevention plan (2011, available on http://www.morbihan.gouv.fr/), which includes a flood hazard assessment (*Le Cornec and Schoorens* 2007; *Le Cornec and Peeters* 2008), they know for instance that there is a risk of flooding when a storm is coming with strong local south wind together with a spring tide. In this case, they monitor several critical locations, mainly along the south beach (Grande Plage), 1 or 2 hours before the high tide of storm arrival. As practical results of our study, we refine this knowledge by estimating the main critical patterns on one hand, based on the DED and HMD databases, on the other hand, based on modelling (for the DEM_{2008} configuration). The analyses of the DED and HMD database provide some values which can be considered as secure ones (since the coastal defences are currently upgraded): $\xi_c = 2.77$ m IGN69, $H_{sc} = 2.6$ m, $T_{pc} = 9$ s, $U_c = 4$ m/s (Figure 8). Similar critical values are found when analysing the model results (ratio r introduced in section 4.2.2, Figure 10): $\xi_c = 2.5$ m IGN69, $H_{sc} = 2$ m, $T_{pc} = 9$ s, $U_c = 5$ m/s. These thresholds are slightly different from those obtained using the DED and HMD databases, keeping in mind that: (1) the discretisation used to compute the ratio r in the forcing parameter space was limited by the number of simulations ($\Delta\xi = 0.25$ m, $\Delta H_s = 1$ m, $\Delta T_p = 1$ s, $\Delta U = 5$ m/s), (2) the simulations used for the analyses were done with a single DEM (2008), (3) the 48 damage events of the database do not cover all the possible hydro-meteorological conditions. First, such similar results imply that knowing only the past hydro-meteorological conditions corresponding to the 48 damage events allows to already tackle the main critical conditions. The additional simulations allow to better capture the joint contours. Second, the model-based estimation of the critical conditions and contours were obtained for the DEM_{2008} configuration, and thus, should be considered as safety conditions. Such estimation could be further refined to better capture the present day contours by: (1) considering the upgraded coastal defences and present topo-bathymetry, (2) increasing the number of simulations. To properly cover the input space, assuming a regular computation grid experiment, a minimum of 10^6 simulations (considering the 6 parameters and 10 values per parameters) would be

needed to estimate the probability of flood in each bivariate space. This would be far too computationally expensive. Therefore, it could be worthwhile to set up a meta-model to better assess the critical contours (see e.g. *Rohmer and Idier* 2012). Such a meta-model could either focus on flood/no flood occurrence, or on the flood indicator Vol. The work of *Azzimonti et al.* (2019) could also be used to visualize such 6D contours. In addition, it would be needed to regularly update the r plots with the evolution of the topo-bathymetry (including coastal defence evolution).

As highlighted by the simulations and the historical 2001 flood event, coastal defences have a significant effect in Gâvres. However, even with the upgraded coastal defences ($\mathrm{DEM}_{upgrade}$), the hydro-meteorological conditions which led to the 1904 and 1924 flood events are associated to flood indicator of the same order of magnitude as the one computed for the Johanna event with the DEM_{2008} configuration (Figure 6). This gives an indication of the minimal potential intensity of flood that could still occur on Gâvres. In addition, these two large events occurred at the beginning of the century, for a lower mean sea level (Figure 9). If such event occurred in 2017 (in 2017, $MSL = 0.53$ m IGN69, after *SHOM* (2017)), their expected impact would be even worse, with a still water level (3.45 and 3.31 m IGN69, respectively) closer to the largest value of the HMD database (Xynthia, 3.47 m IGN69), but with much more energetic wave conditions. The analysis of the changes in joint return period of the water level and the wave height induced by sea-level rise suggests that by 2100, these joint conditions would statistically occur at least once a year. The induced flood will then strongly depend on the risk prevention measures applied in Gâvres. This type of analysis assumes that climate change has a negligible effect on tide (on the study site) and meteorological conditions (which induces atmospheric surge and wave), in comparison with the effect of mean sea-level rise. This assumption seems to be valid at the first order for large enough sea-level rise, based on the work of *Idier et al.* (2017) and *Vousdoukas et al.* (2018). A full integration of the nonstationary character of extreme marine variables is identified as a perspective of the present work and can build on recent advances in multivariate extreme value analysis under nonstationary (see e.g. *Davies et al.* 2017; *Galiatsatou et al.* 2019).

6 Conclusion

In this study, we provide a pluri-disciplinary method relying on history, statistics and modelling to improve our knowledge of past flood events and their driving factors. We apply this approach on the macro-tidal site of Gâvres (French Atlantic coast). Using together historic information (archives, newspapers), hindcasts, hydrodynamic models and local knowledge on the evolution of the territory, we identify 9 flood events on the 1900-2010 period, amongst which 5 significant flood events (4 with high confidence: 1924, 1978, 2001, 2008; 1 with a lower confidence: 1904). The 1904 event was clearly identified owing to the cross-fertilization of the damage and hydro-meteorological databases and the flood simulations. These flood events are driven by the combination of sea-level rise, tide, atmospheric surge, offshore wave conditions and local wind. The patterns of the 1904 and 2008 events significantly differ from those of the 1924 and 1978 events: larger still water level, less energetic waves, and stronger local wind.

The analysis of the hydro-meteorological conditions allows driving the main patterns of the critical contours separating no flood and flood conditions. The analysis of the databases and modelling results lead to very similar conclusions, with the following critical conditions guaranteeing safety against flooding assuming no failure of coastal defences: still water level of ~ 2.5 m IGN69, significant wave height of ~ 2 m, peak period ~ 9 s, wind of ~ 4 m/s. For the events characterised by strong local winds, the local wind direction has a significant effect on the flood intensity. Strictly speaking, these critical conditions apply to the bathymetry and coastal defences up to 2008.

An estimated low bound of return period of significant flood event is estimated to be about 20 years, while the return period of exceedance of the associated still water level (relative to mean sea level) and wave height is ranging between less than 1 y (2001 event) to more than 1000 y (1924 event). However, these return periods are changing due to ongoing sea-level rise. They will fall to values smaller than 1 y for all historical flood events, except that of 1924, under the median sea-level projection of the 5^{th} assessment report of the IPCC. Even if this return period represents the probability of a part of the forcing parameters, this illustrates how the future local coastal defence strategy will be crucial for the study site.

The present analysis is based on 48 damage events, 9 observed flood and about 448 numerical simulations. To really assess flood probability (rather than the probability of forcing conditions) and to improve early-warning systems, more simulations would be needed. Furthermore, accounting for the evolving topo-bathymetry and coastal defences would be necessary. A promising way forward could be the development and use of the meta-model approach (*Rohmer and Idier* 2012; *Rueda et al.* 2016). Finally, accounting for the evolving topo-bathymetry and coastal defences would be necessary to progress in the area of detection and attribution of coastal flood changes.

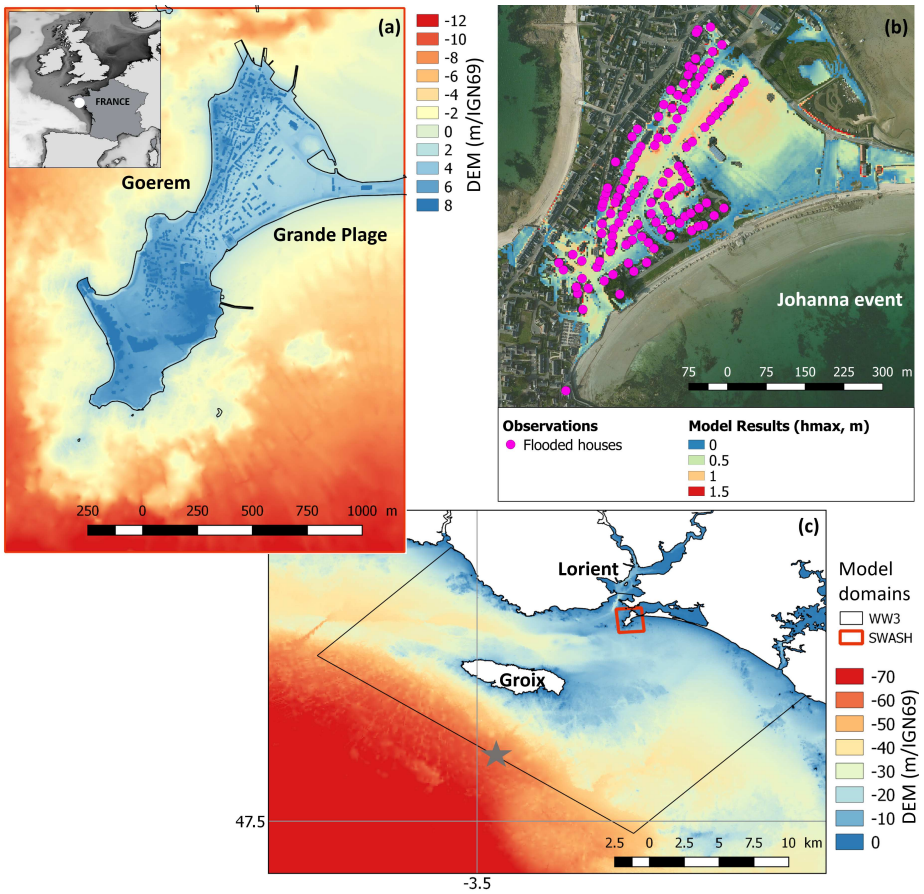

Fig. 1 (a) location of the site and topo-bathymetry; (b) observed and modelled flood for the Johann event (10th March 2018); (c) surrounding of the study site, computational domains of the hydrodynamics models (WGS84) and location of the offshore forcing wave conditions (grey star).

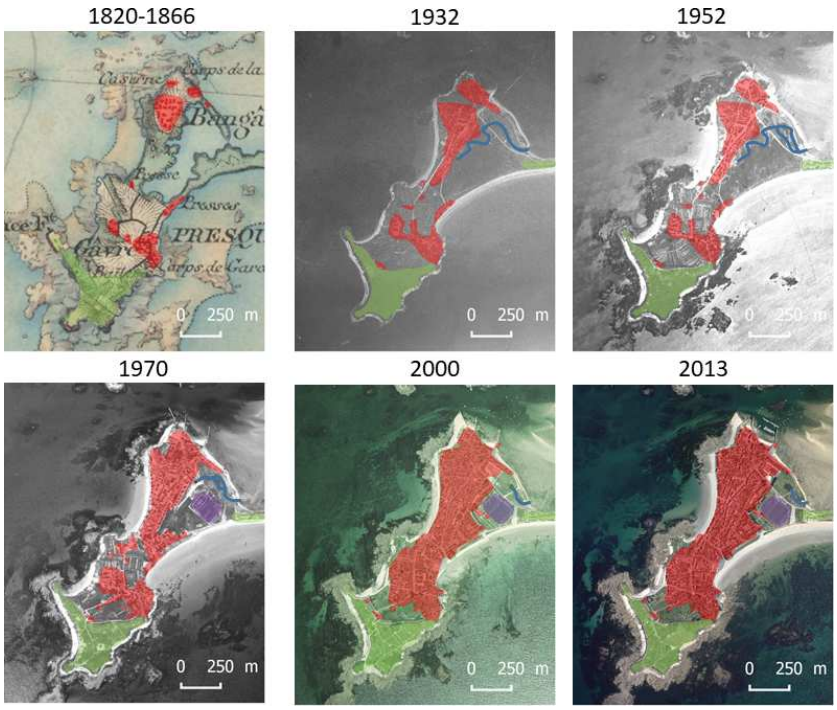

Fig. 2 Time evolution of the land cover: the top-left figure is extracted from the 1820-1866 Etat Major map (the red color indicates buildings). The other aerial photos are provided by IGN (Institut National de l'Information Géographique et Forestière). Green: historical military area, red: civil buildings, purple: sports field.

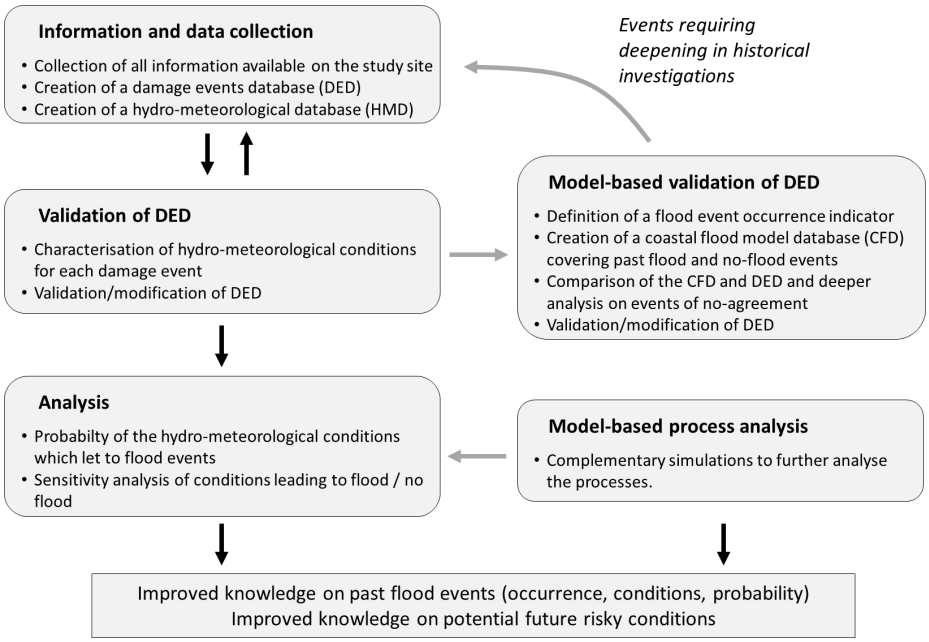

Fig. 3 Flowchart of the method used in the present paper.

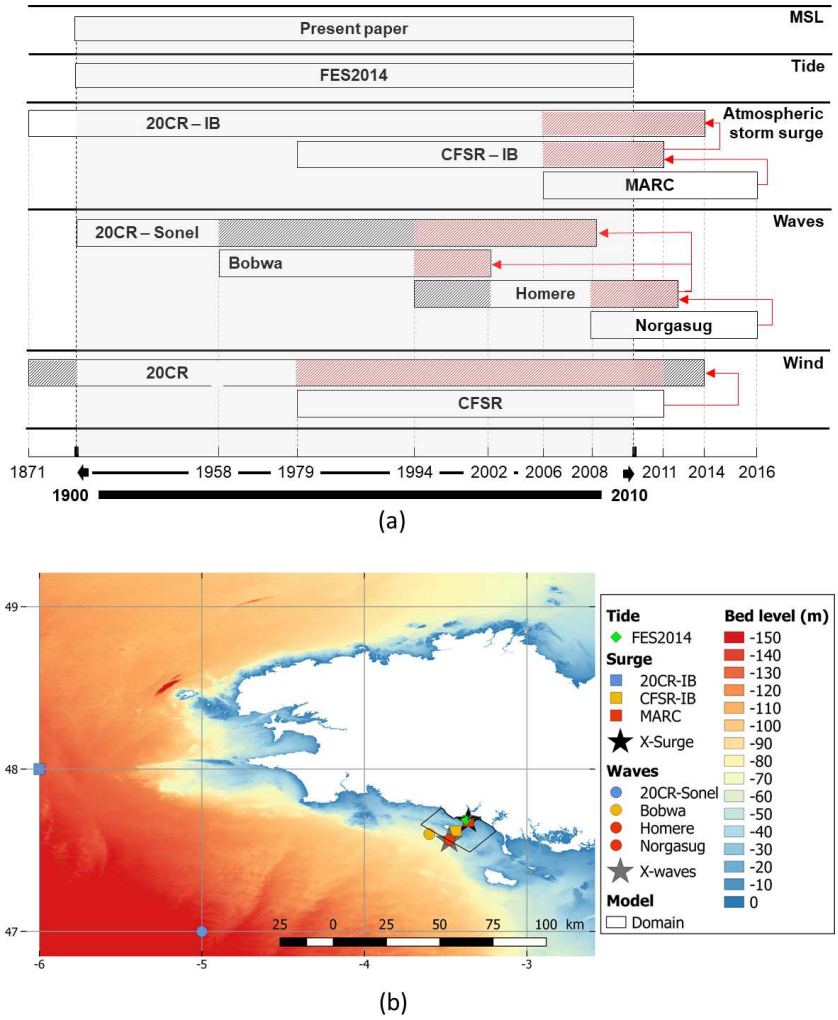

Fig. 4 Hydro-Meteorological Database: (a) data sources (extraction date: 2017), dataset period used to learn the QQ-corrections (in red), final selected dataset (in white). (b) Location of the tide, surge and wave datasets. X-Surge and X-waves indicate the location of the final composite data of surge and waves, respectively, in the Hydro-Meteorological Database. Source of bathymetric data: (*SHOM* 2015).

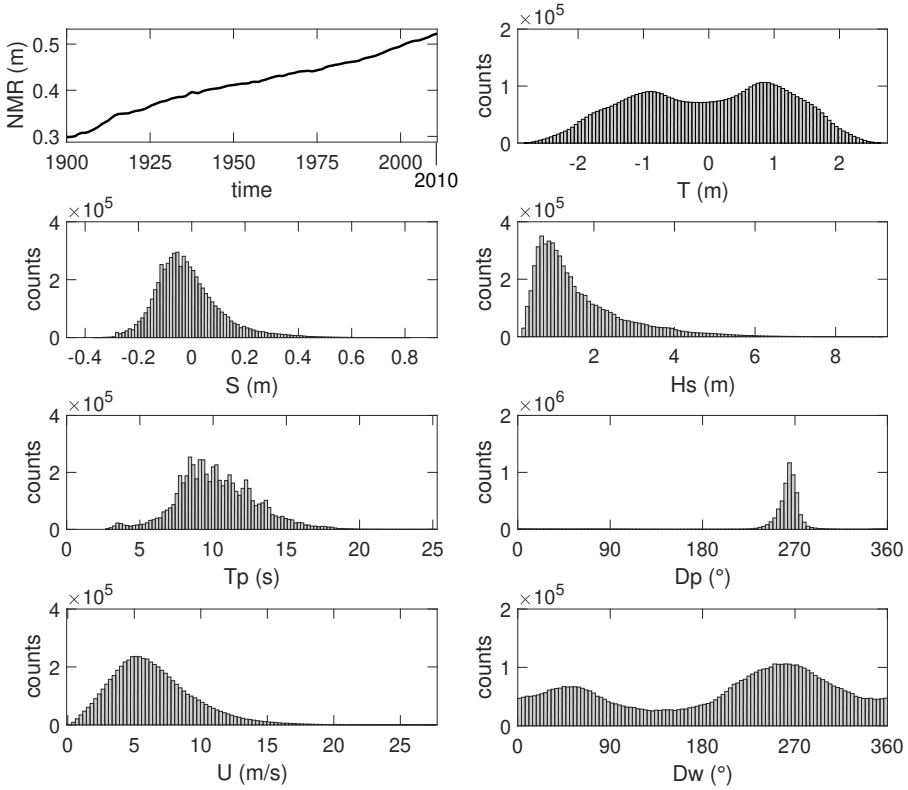

Fig. 5 Hydro-meteorological database: time series of the relative mean sea level (MSL) and distribution of the other hydro-meteorological variables: tide (T), surge (S), significant wave height (H_s), peak period (T_p), peak direction (D_p), wind velocity (U), wind direction (D_u).

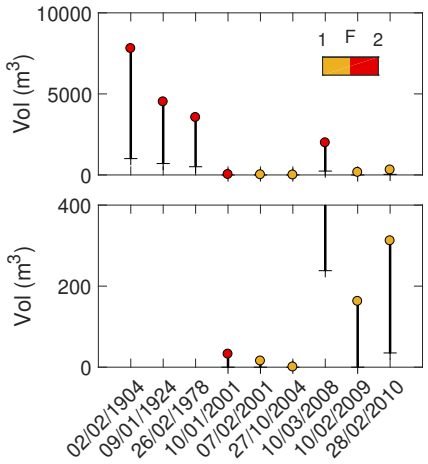

Fig. 6 Simulated flood indicator (Vol) for the 2008 topography (coloured points, DEM_{2008}) and the upgraded coastal defence case (+, $\mathrm{DEM}_{upgrade}$), considering the events with $F \geq 1$. The colors refer to the Flood value of the Damage database. The bottom panel is a zoom of the upper panel for Vol values close to zero.

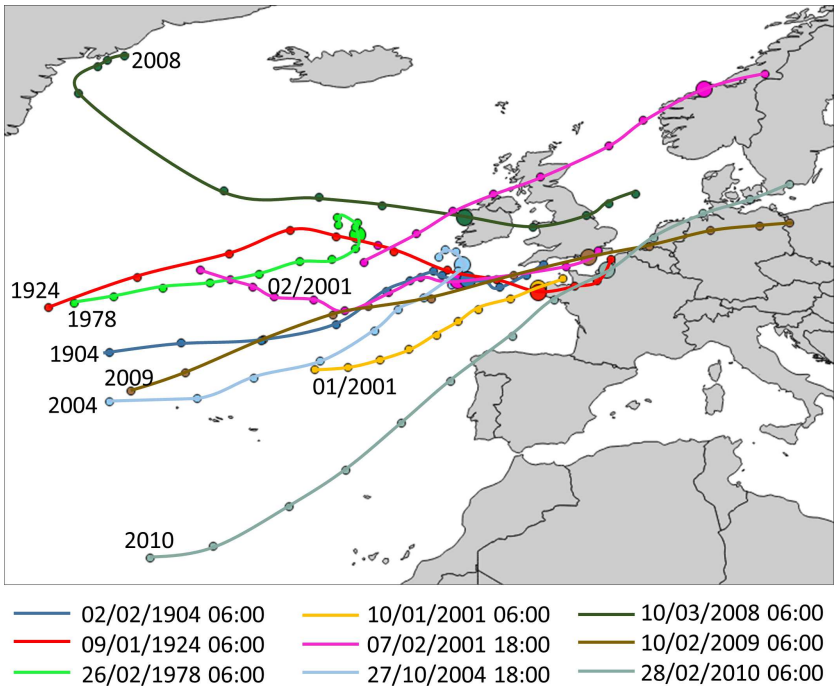

Fig. 7 Storm tracks associated with the 9 flood events, based on the 500hPa geopotential pressure, extracted from the 20CR data (until 1978), and CFSR data (after 1978), every 6 hours. Dates in caption indicate the reference time (large size circle).

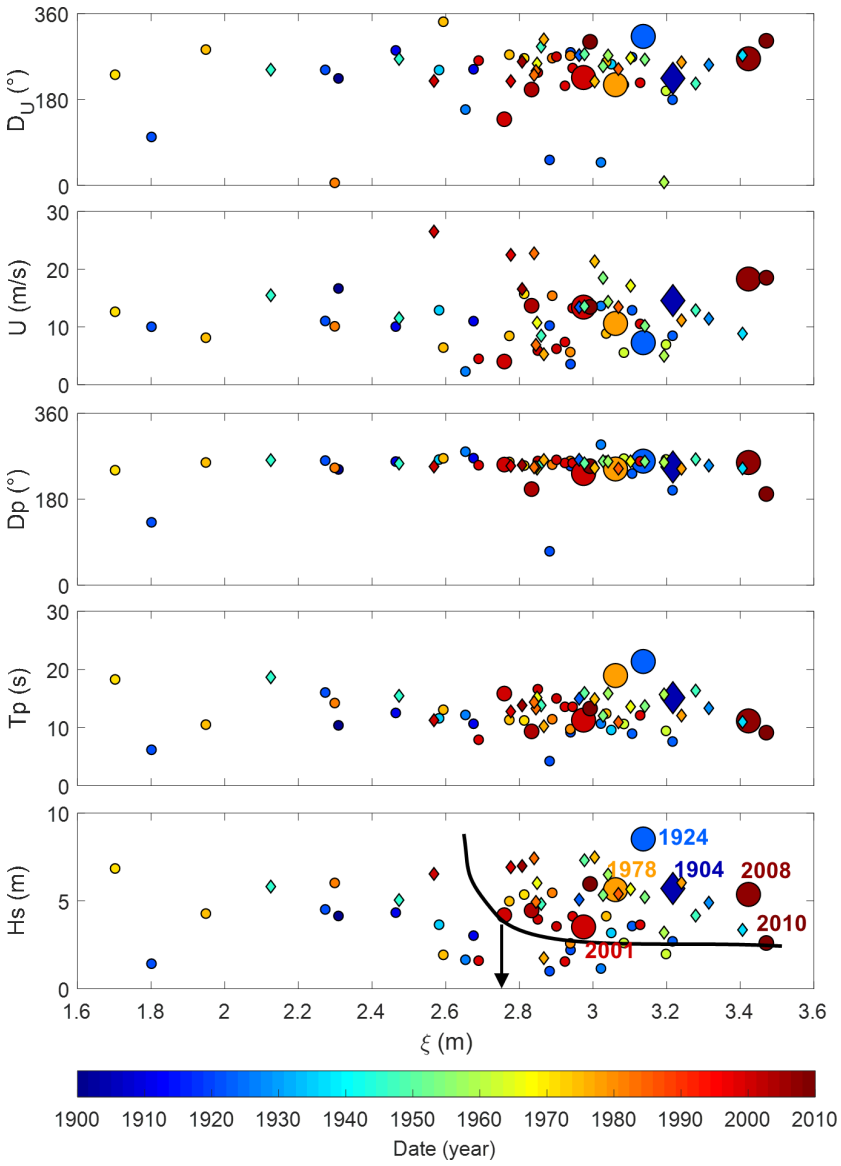

Fig. 8 Scatter plot of the Hydro-Meteorological conditions of the events of the Damage Event Database. The black arrow (bottom panel) indicates the smallest still water level (ξ_c=2.77 m IGN69) among the flood events ($F \geq 1$). The marker size indicates the *Flood* value (0-no flood: small size, 1-moderate flood: medium size, 2-significant flood: large size). The symbols indicate the confidence indicator value (1-medium confidence: diamond, 2-high confidence: circle). Years of the 5 main flood events are indicated. The grey areas indicate cluster of main flood ($F = 2$) event types. The black contour indicates an approximation of the critical contour so that an event can cause flooding only if it is associated with values above this contour.

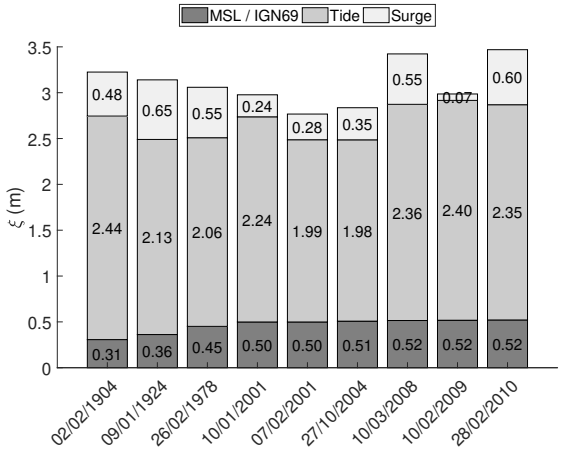

Fig. 9 Contribution of each water level component to the still water level (ξ), for the 9 flood events.

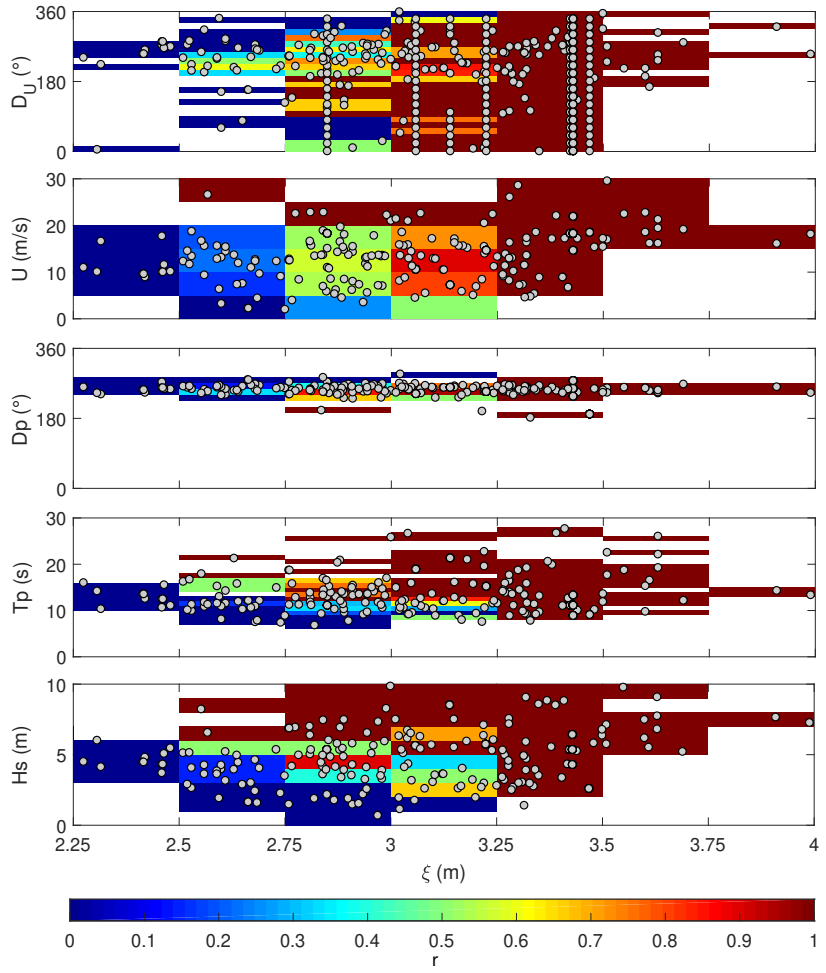

Fig. 10 Identification of conditions leading to flooding, based on the numerical flood simulations. The color scale indicates the value of the ratio r between the number of simulations providing $Vol > 0$ and the total number of computations for in each cell. Dots: simulation points. Based on simulations done with the DEM_{2008}.

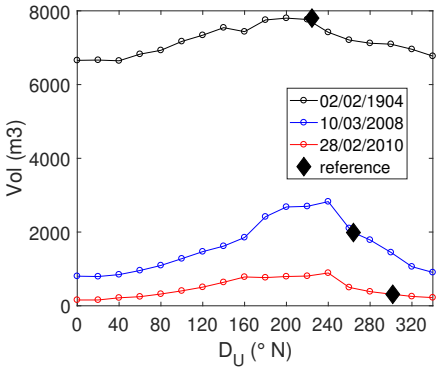

Fig. 11 Sensitivity of the flood indicator Vol to the wind direction D_u for the 3 flood events of largest wind speed, for the DEM_{2008} configuration.

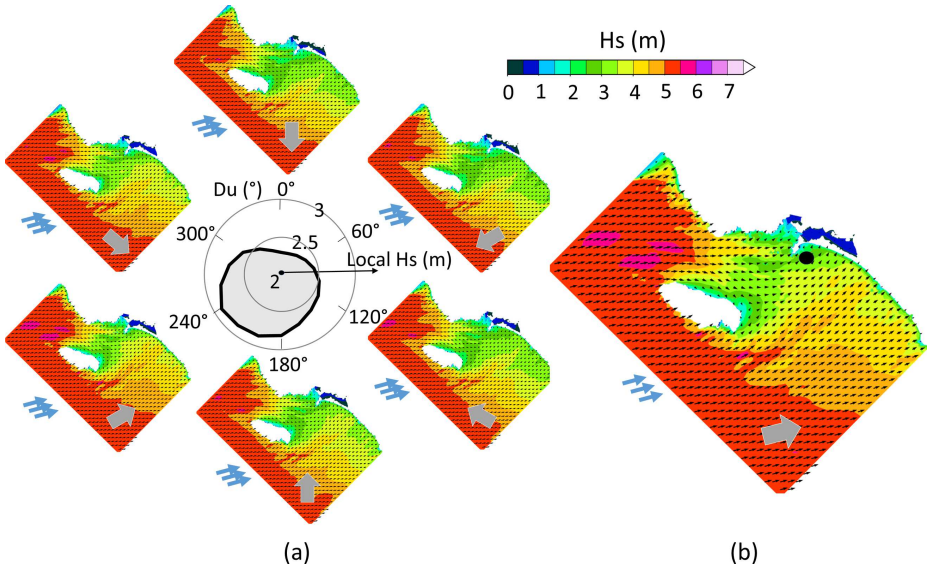

Fig. 12 WW3 model results (H_s) for the hydro-meteorological conditions corresponding to the Johanna event (b, $D_u = 264°$), and for the same event, but for different wind directions (a, $D_u = 0$, 60, 120, 180, 240, 300°). The polar plot indicates the significant wave height close to Gâvres (black dot on the right panel) for $D_u = 0{:}20{:}340°$. Grey arrows indicate the wind direction and blue arrows the offshore wave direction ($D_p = 255°$ for the Johanna event).

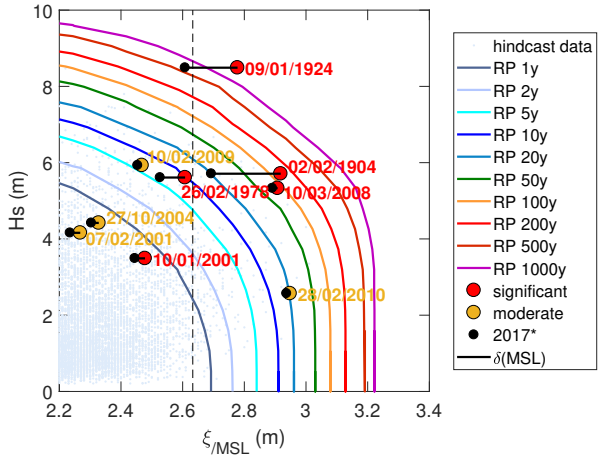

Fig. 13 Joint exceedance contours within the space $(\xi_{/MSL}, H_S)$ for return period values ranging from 10 to 1000 years together with the nine historical events. Note that the still water level $\xi_{/MSL}$ is expressed with respect to the mean sea level, i.e. $\xi_{/MSL} = \xi - MSL$. The flood events of the damage database are indicated with coloured markers. The 2017* markers indicate the value of $\xi_{/MSL}$ of each event in case the same total still water level would occur in 2017 (i.e. $\xi_{/MSL_{2017}} = \xi_{/MSL_{event}} - \delta(MSL)$ with $\delta(MSL) = MSL_{2017} - MSL_{event}$ and *event* refers to the selected event).

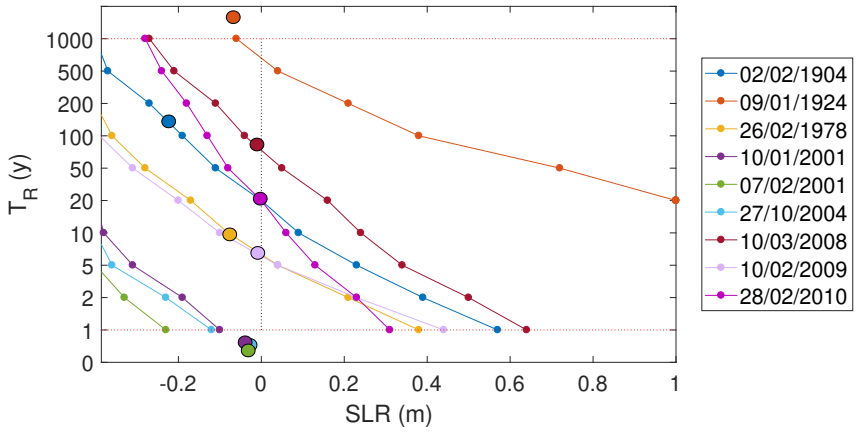

Fig. 14 Return periods T_R of the 9 flood events as a function of the mean sea-level rise (SLR). $SLR = 0$ corresponds to the year 2017 (vertical dotted line). The large circles indicate the return period T_R corresponding to the past events.

Table 1 Original datasets of tide, surge, waves and winds for the hydro-meteorological database. The asterisk (*) indicates that there is a data transformation (in the present case, sea surface pressure data are extracted and converted in storm surges using the inverse barometer computation). Websites: 1 (https://www.aviso.altimetry.fr/en/data/products/auxiliary-products/global-tide-fes/description-fes2014.html), 2 (https://reanalyses.org/atmosphere), 3 (https://climatedataguide.ucar.edu/climate-data/climate-forecast-system-reanalysis-cfsr), 4 (http://marc.ifremer.fr/), 5 (http://www.sonel.org/-Waves-.html?lang=en), 6 (http://bobwa.brgm.fr/), 7 (http://marc.ifremer.fr/en/produits/rejeu_d_etats_de_mer_homere), 8 (https://wwz.ifremer.fr/iowaga/Products)

Parameter	Source			
	Name	Provider	Reference	Website
Tide (T)	FES2014	LEGOS	Carrere et al. (2016)	1
Storm surge (S)	20CR*	NOAA	Compo et al. (2015)	2
	CFSR*	NOAA	Dee et al. (2014)	3
	MARC	Ifremer-LOPS	Muller et al. (2014)	4
Waves (Hs,Tp,Dp)	Sonel (waves)	Liens	Bertin et al. (2013)	5
	BoBWA	BRGM	Charles et al. (2012)	6
	Homere	Ifremer-LOPS	Boudière et al. (2013)	7
	Norgasug	Ifremer-LOPS	Boudière et al. (2013)	8
Wind (U,Dw)	20CR	NOAA	Compo et al. (2015)	2
	CFSR	NOAA	Dee et al. (2014)	3

Table 2 Sources for the 9 flood events of the final Damage Database (after update). For the First half century, all the newspaper are available in the "Archives Départementales du Morbihan". Most of them have been gathered in (*Lambert* 2017). The newspaper articles used in this study after 1950 come from (*Le Cornec et al.* 2012). In what follows, the following specific archives also used (extracted from (*Le Cornec et al.* 2012)): ADM1 (Archives Départementales du Morbihan / rapport du Subdivisionnaire, pour la demande de crédit pour les réparations des avaries causées aux cales de Larmor et de Gâvres par la tempête du 27 Novembre 1924, 15 décembre 1924), CELM1 (Centre d'Essai de Lancement de Missiles / Relevé des tempêtes majeures sur le polygone de Gâvres), Cetmef1 (Cetmef Février 2001), GT (Gâvres town hall / Délibération du Conseil Municipal du 24 janvier 2001), SHM1 (Service Historique de La Marine / courrier du Président de la Commission de Gâvres au Préfet maritime de Lorient, 09/05/1904), SHM2 (Service Historique de La Marine / Consolidation de l'ouvrage de protection du rivage, Tranche 1978, Notice explicative).

Damage Event Nd (date)	Sources
2 (02/02/1904)	Courrier Morbihannais 7/02/1904 ; Le Matin 05/02/1904
	Courrier des Campagnes 7/02/1904 ; L'Arvor 05/02/1904
	La Croix du Morbhian 14/02/1904 ; SHM1
7 (09/01/1924)	Nouvelles de Lorient 29/11/1924
	Le Nouvelliste du Morbihan 30/11/1924
	L'ouest Républican 30/11/1924 and 04/12/1924 ; ADM1
29 (26/02/1978)	CELM1 ; SHM2
42 (10/01/2001)	Le Télégramme 11 and 12/01/2001
	Ouest France 11/01/2001 ; GT1
43 (07/02/2001)	Cetmef1
44 (27/10/2004)	Le Télégramme 29/10/2004
46 (10/03/2008)	Le Télégramme 11/03/2008 ; Ouest France 11/03/2008
	Le Cornec et al. (2012)
47 (10/02/2009)	Ouest France 11/02/2009 ; *Le Cornec et al.* (2012)
48 (28/02/2010)	*Le Cornec et al.* (2012)

Table 3 List of the 9 flood events of the damage database, the corresponding Hight Tide time (Universal Time) and the corresponding hydro-meteorological conditions extracted (at high tide) from the HMD database (MSL: mean sea level, T: tide, S: atmospheric storm surge, H_s: significant wave height, T_p: wave peak period, D_p: wave peak direction, U: wind speed, Du: wind direction). The significant flood events and the maximum values (among the 9 events) of intensity parameters (i.e. MSL, T, S, H_s and U) are given in bold.

Event	HT	MSL (m)	T (m)	S (m)	Hs (m)	Tp (s)	Dp (°)	U (m/s)	Du (°)
02/02/1904	04:00	0.307	2.438	0.48	5.71	15.1	247.6	14.6	224.4
09/01/1924	05:30	0.362	2.128	**0.65**	**8.49**	**21.3**	258.5	7.8	310.8
26/02/1978	05:30	0.451	2.058	0.55	5.61	18.8	242.0	10.5	209.7
10/01/2001	03:40	0.499	2.238	0.24	3.49	11.2	232.6	13.3	224.7
07/02/2001	15:20	0.499	1.988	0.28	4.16	15.7	251.3	3.9	137.4
27/10/2004	15:20	0.508	1.978	0.35	4.42	9.23	199.9	13.6	199.6
10/03/2008	05:20	0.515	2.358	0.55	5.33	11.0	255.7	18.2	264.1
10/02/2009	04:00	0.518	**2.398**	0.07	5.93	13.2	248.0	13.4	299.6
28/02/2010	03:10	**0.521**	2.348	0.60	2.57	9.0	189.7	**18.4**	301.7

Acknowledgements The authors thank the ANR for its financial support to the RISCOPE project (ANR-16-CE04-0011). The following data providers are acknowledged: LEGOS, NOAA, LOPS-IFREMER, SHOM. X. Bertin is also acknowledged for having running and provided the Sonel-waves data. T. Bulteau is acknowledged for discussions on the implementation of the method of *Heffernan and Tawn* (2004). The authors are also grateful to local stakeholders comity of the RISCOPE project which provided useful informal knowledge and some key reports and data (D. Le Vouédec, M.O. Botti-Le-Formal), to L. Pineau-Guillou and C. Meur-Ferec for fruitful discussions, and to the anonymous referee for his insightful comments that strengthened this paper.

References

Aarnes J.E., Krogstad H.E. (2001) Partitioning sequences for the dissection of directional ocean wave spectra: A review. Part of work package 4 (Wp4) of the EnviWave (EVG-2001-00017) research programme under the EU Energy, Environment and Sustainable Development programme.

André C. (2014) Analyse des dommages liés aux submersions marines et évaluation des coûts induits aux habitations à partir de données d'assurance : perspectives apportées par les tempêtes Johanna (2008) et Xynthia (2010). PhD Manuscript. Géographie. Université de Bretagne occidentale - Brest, 2013. Français.

Ardhuin F., Rogers W.E., Babanin A.V., Filipot J., Magne R., Roland A., Van der Westhuysen A., Queffeulou P., Lefevre J., Aouf L., Collard F. (2010) Semiempirical dissipation source functions for ocean waves. Part I: Definition, calibration, and validation. J. Phys. Oceanogr. 40(1), 917– 1,941.

Arns A., Wahl T., Dangendorf S., Jensen J. (2015) The impact of sea level rise on storm surge water levels in the northern part of the German Bight. Coastal Engineering, 96, 118-131.

Azzimonti D., Ginsbourger D., Rohmer J., Idier D. (2019) Profile extrema for visualizing and quantifying uncertainties on excursion regions. Application to coastal flooding. Technometrics, 1-26.

Bertin, X., E. Prouteau, and C. Letetrel (2013) A significant increase in wave height in the North Atlantic Ocean over the 20th century. Global and Planetary Change 106, 77-83.

Bertin X., Li K., Roland A., Zhang Y. J., Breilh J.F., Chaumillon E. (2014) A modeling-based analysis of the flooding associated with Xynthia, central Bay of Biscay. Coastal Engineering 94, 80-89.

Boudiere E., Maisondieu C., Ardhuin F., Accensi M., Pineau-Guillou L., Lepesqueur J. (2013) A suitable metocean hindcast database for the design of Marine energy converters. International Journal of Marine Energy, 3-4, e40-e52. doi:j.ijome.2013.11.010.

Breilh J.F.., Bertin X., Chaumillon E., Giloy N., Sauzeau T. (2014) How frequent is storm-induced flooding in the central part of the Bay of Biscay?, Global and Planetary Change, 122, 161–175.

Bulteau T., Idier D., Lambert J., Garcin M. (2015) How historical information can improve estimation and prediction of extreme coastal water levels: application to the Xynthia event at La Rochelle (France), Nat. Hazards Earth Syst. Sci., 15, 1135–1147.

Cariolet J.M. (2011) Inondation des côtes basses et risques associés en Bretagne : vers une redéfinition des processus hydrodynamiques liés aux conditions météo-océaniques et des paramètres morphosédimentaires. Océan, Atmosphère. Université de Bretagne occidentale - Brest, 2011. Français. <tel-00596426>.

Carrere L., F. Lyard, M. Cancet, A. Guillot, N. Picot (2016) FES 2014, a new tidal model - Validation results and perspectives for improvements, presentation to ESA Living Planet Conference, Prague.

Carson M., Köhl A., Stammer D., Slangen A.B.A., Katsman C.A., Van de Wal R.S.W., Church J., White N. (2016) Coastal sea level changes, observed and projected during the 20th and 21st century. Climatic Change, 134(1-2), 269-281.

Church J.A., P.U. Clark, A. Cazenave, J.M. Gregory, S. Jevrejeva, A. Levermann, M.A. Merrifield, G.A. Milne, R.S. Nerem, P.D. Nunn, A.J. Payne, W.T. Pfeffer, D. Stammer and A.S. Unnikrishnan (2013) Sea Level Change. In: Climate Change 2013: The Physical Science Basis. Contribution of Working Group I to the Fifth Assessment Report of the Intergovernmental Panel on Climate Change [Stocker, T.F., D. Qin, G.-K. Plattner, M. Tignor,

894 S.K. Allen, J. Boschung, A. Nauels, Y. Xia, V. Bex and P.M. Midgley (eds.)]. Cambridge
895 University Press, Cambridge, United Kingdom and New York, NY, USA.
896 Coles S.G., Tawn J.A. (1991) Modelling extreme multivariate events. J. R. Stat. Soc. Ser. B
897 Methodol. 53 (2), 377–392.
898 Coles S. (2001). An Introduction to StatisticalModelling of Extreme Values. Springer series in
899 statistics.
900 Compo G.P., Whitaker J.S., Sardeshmukh P.D., Allan R.J., McColl C., Yin X., Giese B.S.,
901 Vose R.S., Matsui N., Ashcroft L., Auchmann R., Benoy M., Bessemoulin P., Brandsma T.,
902 Brohan P., Brunet M., Comeaux J., Cram T., Crouthamel R., Groisman P.Y., Hersbach
903 H., Jones P.D., Jonsson T., Jourdain S., Kelly G., Knapp K.R., Kruger A., Kubota H.,
904 Lentini G., Lorrey A., Lott N., Lubker S.J., Luterbacher J., Marshall G.J., Maugeri M.,
905 Mock C.J., Mok H.Y., Nordli O., Przybylak R., Rodwell M.J., Ross T.F., Schuster D.,
906 Srnec L., Valente M.A., Vizi Z., Wang X.L., Westcott N., Woollen J.S., Worley S.J. (2015)
907 NOAA/CIRES Twentieth Century Global Reanalysis Version 2c. Research Data Archive
908 at the National Center for Atmospheric Research, Computational and Information Systems
909 Laboratory. https://doi.org/10.5065/D6N877TW. Accessed 28 feb 2017.
910 Corriou J.P. (2012) Commande des procédés, 1–766, Lavoisier, Tec& Doc.
911 Dangendorf S., Arns A., Pinto J.G., Ludwig P., Jensen J. (2016) The exceptional influence
912 of storm 'Xaver' on design water levels in the German Bight. Environmental Research
913 Letters, 11(5), p.054001.
914 Davies G., Callaghan D. P., Gravois U., Jiang W., Hanslow D., Nichol S., Baldock T. (2017)
915 Improved treatment of non-stationary conditions and uncertainties in probabilistic models
916 of storm wave climate. Coastal Engineering, 127, 1-19.
917 Dee D.P., Balmaseda M., Balsamo G., Engelen R., Simmons A.J., Thépaut J.-N. (2014) Toward
918 a Consistent Reanalysis of the Climate System. Bull. Amer. Meteor. Soc., 95, 1235–1248.
919 Fortunato A.B., Freire P., Bertin X., Rodrigues M., Ferreira J., Liberato M.L. (2017) A numer-
920 ical study of the February 15, 1941 storm in the Tagus estuary. Continental Shelf Research
921 144, 50-64.
922 Galiatsatou P., Makris C., Prinos P., Kokkinos D. (2019) Nonstationary joint probability
923 analysis of extreme marine variables to assess design water levels at the shoreline in a
924 changing climate. Natural Hazards, 98(3), 1051-1089.
925 Gallien T.W., Kalligeris N., Delisle M.P.C., Tang B.X., Lucey J.T.D., Winters M.A. (2018)
926 Coastal Flood Modeling Challenges in Defended Urban Backshores. Geosciences 8, 450,
927 10.3390/geosciences8120450.
928 Garnier E., Ciavola P., Spencer T., Ferreira O. Armaroli C., Mc Ivor A. (2018) Historical
929 analysis of storm events: Case studies in France, England, Portugal and Italy. Coastal
930 Engineering, 134, 0-23.
931 Garrity N. J., Battalio R., Hawkes P. J., Roupe D. (2007) Evaluation of event and response
932 approaches to estimate the 100-year coastal flood for Pacific coast sheltered waters. Coastal
933 Engineering, 1651-1663.
934 Giloy N., Hamdi Y., Bardet L., Garnier E., Duluc C. M. (2018) Quantifying historic skew
935 surges: an example for the Dunkirk Area, France. Natural Hazards, 1-25.
936 Gouldby B., Méndez F.J., Guanche Y., Rueda A., Mínguez R. (2014). A methodology for
937 deriving extreme nearshore sea conditions for structural design and flood risk analysis.
938 Coastal Engineering, 88, 15-26.
939 Gudmundsson L., Bremnes J. B., Haugen J. E., Engen-Skaugen T. (2012) Technical Note:
940 Downscaling RCM precipitation to the station scale using statistical transformations - a
941 comparison of methods. Hydrology and Earth System Sciences, 16, 3383-3390.
942 Haigh I.D., Nicholls R.J., Wells N. (2011) Rising sea levels in the English Channel 1900 to
943 2100. Proceedings of the Institution of Civil Engineers - Maritime Engineering, 164(2),
944 81-92.
945 Haigh I., Wadey M.P., Wahl T., Ozsoy O., Nicholls R.J., Brown J.M., Horsburgh K., Gouldby
946 B. (2016) Spatial and temporal analysis of extreme sea level and storm surge events around
947 the coastline of the UK. Scientific Data, 3, 160107.
948 Haigh I.D., Ozsoy O., Wadey M.P., Nicholls R.J., Gallop S.L., Wahl T., Brown,, J.M. (2017)
949 An improved database of coastal flooding in the United Kingdom from 1915 to 2016.
950 Scientific data, 4, 170100.
951 Hallegatte S., Green C., Nicholls R.J., Corfee-Morlot, J. (2013) Future flood losses in major
952 coastal cities. Nature climate change, 3(9), 802.

Hamdi Y., Garnier E., Giloy N., Duluc C. M., Rebour V. (2018) Analysis of the risk associated with coastal flooding hazards: a new historical extreme storm surges dataset for Dunkirk, France. Natural Hazards and Earth System Sciences, 18(12), 3383-3402.

Hawkes P. J., Gouldby B. P., Tawn J. A., Owen M. W. (2002) The joint probability of waves and water levels in coastal engineering design, J. Hydraul. Res., 40, 241–251.

Heffernan J.E., Tawn J.A. (2004) A conditional approach for multivariate extreme values (with discussion). J. R. Stat. Soc. Ser. B Stat Methodol. 66 (3), 497–546.

Hénaff A., Le Cornec E., Jabbar M., Pétré A., Corfou J., Le Drezen Y., Van Vliët-Lanoë B. (2018) Caractérisation des aléas littoraux d'érosion et de submersion en Bretagne par l'approche historique, Cybergeo: European Journal of Geography, 847.

Jevrejeva S., Moore J.C., Grinsted A., Matthews A.P., Spada G. (2014) Trends and acceleration in global and regional sea levels since 1807. Global and Planetary Change, 113, 11-22.

Idier D., Muller H., Pedreros R., Thiébot J., Yates M., avec la collaboration de Créach R., Voineson G., Dumas F., Lecornu F., Pineau-Guillou L., Ohl P., Paradis D. (2012) Système de prévision de surcotes en Manche/Atlantique et Méditerranée : Amélioration du système existant sur la façade Manche/Gascogne [D4]. Rapport final. BRGM/RP-61019-FR, 165 p., 71 fig., 11 tabl., 9 ann.

Idier D., Rohmer J., Bulteau T., and Delvallée E. (2013) Development of an inverse method for coastal risk management, Nat. Hazards Earth Syst. Sci., doi:10.5194/nhess-13-999-2013, 13, 999–1013.

Idier D., Paris F., Le Cozannet G., Boulahya F., Dumas F. (2017) Sea-level rise impacts on the tides of the European Shelf, Continental Shelf Research.

Jeffers J.M. (2014) Environmental knowledge and human experience: using a historical analysis of flooding in Ireland to challenge contemporary risk narratives and develop creative policy alternatives. Environmental Hazards, 13(3), 229-247.

Lambert J. (2017) Contribution au recensement des effets de tempêtes historiques dans la région de Gâvres-Lorient (Morbihan). Technical report BRGM_DRP-RSV 17-NT-058.

Le Berre I., David L., Henaff A., Meur-Ferec C., Cuq V., Lageat Y. (2012) Atlas des risques d'érosion - submersion; contribution à l'étude de la vulnérabilité côtière des communes de Gâvres et Guissény. Rapport final Adaptalitt, GICC, LETG-Geomer, UBO, 55 pp.

Le Cornec E., Ferrand J.P. (2009) Etude de protection du littoral de Gâvres. Phase 1 : Analyse des données existantes. GEOS-AEL, Ferrand and DHI report. Lorient-Agglomération, 62 pp.

Le Cornec E., Schoorens G. (2007) Etude de l'aléa submersion marine sur le site de la Grande Plage de Gâvres, Rapport d'étude GEOS-DHI, DDE du Morbihan, 102 pp.

Le Cornec E., Peeters P. (2008) Simulation de la tempête du 10 mars 2008 sur le site de la Grande Plage de Gâvres, Rapport d'étude GEOS-DHI, DDE du Morbihan.

Le Cornec E. and Peeters P. (2010) Etude de l'aléa submersion à Gâvres, in "La gestion du trait de côte", Ministère de l'Ecologie, de l'Energie, du Développement Durable et de la Mer, Editions Quae, pp 238-244. ISBN: 978-2-7592-0360-4.

Le Cornec E., Le Bris E., Van Lierde M. (2012) Atlas des risques littoraux sur le département du Morbihan. Phase 1 : Recensement et conséquences des tempêtes et coups de vent majeurs. Rapport d'étude GEOS-DHI. Direction Départementales des Territoires et de la Mer du Morbihan, 476 pp.

Le Cozannet G., Rohmer J., Cazenave A., Idier D., van De Wal R., De Winter R., Pedreros R., Balouin Y., Vinchon C., Oliveros C. (2015) Evaluating uncertainties of future marine flooding occurrence as sea-level rises. Environmental Modelling and Software, 73, 44-56.

Le Roy S., Pedreros R., André C., Paris F., Lecacheux S., Marche F., Vinchon C. (2015) Coastal flooding of urban areas by overtopping: dynamic modelling application to the Johanna storm (2008) in Gâvres (France), Nat. Hazards Earth Syst. Sci., 15, 2497-2510, https://doi.org/10.5194/nhess-15-2497-2015.

Meyssignac B., Becker M., Llovel W., Cazenave A. (2012) An assessment of two-dimensional past sea level reconstructions over 1950–2009 based on tide-gauge data and different input sea level grids. Surveys in Geophysics, 33(5), 945-972.

Muis S., Verlaan M., Winsemius H.C., Aerts J.C.J.H., Ward P.J. (2016) A global reanalysis of storm surges and extreme sea levels. Nature Communications 7, 11969.

Muller H. Pineau-Guillou L., Idier D., Ardhuin F. (2014) Atmospheric storm surge modeling along the French (Atlantic and English Channel). Ocean Dynamics 64(11):1671-1692.

Needham H.F., Keim B.D. (2012) A storm surge database for the US Gulf Coast. International Journal of Climatology, 32(14), 2108-2123.

Nicolae-Lerma A., Bulteau T., Elineau S., Paris F., Durand P., Anselm, B., Pedreros,R. (2018) High-resolution marine flood modelling coupling overflow and overtopping processes: framing the hazard based on historical and statistical approaches, Nat. Hazards Earth Syst. Sci., 18, 207-229.

Poitevin C., Wöppelmann G., Raucoules D., Le Cozannet G., Marcos M., Testut L. (2019) Vertical land motion and relative sea level changes along the coastline of Brest (France) from combined space-borne geodetic methods. Remote Sensing of Environment, 222, 275-285.

Poulter B., Halpin P.N. (2008) Raster modelling of coastal flooding from sea-level rise. International Journal of Geographical Information Science,22(2), 167–182.

Rohmer J, Idier D (2012) A meta-modelling strategy to identify the critical offshore conditions for coastal flooding, Nat. Hazards Earth Syst. Sci., 12, 2943-2955, https://doi.org/10.5194/nhess-12-2943-2012.

Rohmer J., Le Cozannet G. (2019) Dominance of the mean sea level in the high-percentile sea levels time evolution with respect to large-scale climate variability: a Bayesian statistical approach, Environmental Research Letters, 10.1088/1748-9326/aaf0cd.

Rueda A., Gouldby B., Méndez F. J., Tomás A., Losada I. J., Lara J. L., Díaz-Simal P. (2016) The use of wave propagation and reduced complexity inundation models and metamodels for coastal flood risk assessment. Journal of Flood Risk Management, 9(4), 390-401.

Santamaría-Gómez A., Gravelle M., Collilieux X., Guichard M., Martin-Miguez B., Tiphaneau P., Woppelmann G. (2012) Mitigating the effects of vertical land motion in tide gauge records using a state-of-the-art GPS velocity field. Global and Planetary Change, 98-99, 6-17.

Santamaría-Gómez A., Gravelle M., Dangendorf S., Marcos M., Spada G., Wöppelmann G. (2017) Uncertainty of the 20th century sea-level rise due to vertical land motion errors. Earth and Planetary Science Letters, 473, 24-32.

Sanuy M., Jiménez J. A., Ortego M. I., Toimil A. (2019) Differences in assigning probabilities to coastal inundation hazard estimators: Event versus response approaches. Journal of Flood Risk Management, e12557.

SHOM (2014) Références Altimétriques Maritimes - édition 2014. ISBN 0180-989X.

SHOM (2015) MNT Bathymétrique de façade Atlantique (Projet Homonim). http://dx.doi.org/10.17183/MNT-ATL100m-HOMONIM-WGS84.

SHOM (2017) Références Altimétriques Maritimes - édition 2017. ISBN 978-2-11-139469-8.

Simon B. (1994) Statistique des niveaux marins extremes le long des côtes de France, SHOM Rapport no. 001/94.

Visser H., Dangendorf S., Petersen A.C. (2015) A review of trend models applied to sea level data with reference to the "acceleration-deceleration debate". Journal of Geophysical Research: Oceans, 120(6), 3873-3895.

Vousdoukas M.I., Mentaschi L., Voukouvalas E., Verlaan M., Jevrejeva S., Jackson L.P., Feyen L. (2018) Global probabilistic projections of extreme sea levels show intensification of coastal flood hazard, Nature Communications 9, 2360.

Wadey M.P., Nicholls R.J., Haigh, I (2013) Understanding a coastal flood event: the 10th March 2008 storm surge event in the Solent, UK. Natural Hazards 67, 829–854.

Wadey M., Brown S., Nicholls R.J., Haigh I. (2017) Coastal flooding in the Maldives: an assessment of historic events and their implications. Natural Hazards, 89(1), 131-159.

Wahl T., Haigh I.D., Nicholls R.J., Arns A., Dangendorf S., Hinkel J., Slangen A.B. (2017) Understanding extreme sea levels for broad-scale coastal impact and adaptation analysis. Nature communications, 8, 16075.

Willett P. (1999) Dissimilarity-based algorithms for selecting structurally diverse sets of compounds. J. Comput. Biol. 6 (3–4), 447–457.

Wöppelmann G., Marcos M. (2016) Vertical land motion as a key to understanding sea level change and variability. Reviews of Geophysics, 54(1), 64-92.

Zijlema M., Stelling G., Smit P. (2011) SWASH: An operational public domain code for simulating wave fields and rapidly varied flows in coastal waters. Coast. Eng. 58:992-1012.

Zong Y., Tooley M.J. (2003) A Historical Record of Coastal Floods in Britain: Frequencies and Associated Storm Tracks, Natural Hazards, 29, 13–36.

A Reconstruction of past sea-level changes in the Bay of Biscay and Gâvres

A.1 Reconstruction of past sea-level changes in the Bay of Biscay

We follow the approach of *Rohmer and Le Cozannet* (2019) to reconstruct past geocentric mean sea-level changes in the Bay of Biscay. This approach assumes that once vertical ground motions are removed, all tide gauge measure the same geocentric mean sea-level changes along the coasts of the Bay of Biscay. The approach uses data from PSMSL (Permanent Service for Mean Sea-Level) and SONEL (*Santamaría-Gómez et al.* 2012, www.sonel.org) and proceeds as follows:

- First, we compute relative mean sea-level changes and their uncertainties using a forward-backward Kalman filter (*Corriou* 2012; *Visser et al.* 2015) at the following tide gauge: Devonsport, Newlyn, St Mary, Roscoff Le Conquet, Brest, St Nazaire, Les Sables D'Olonne, La Rochelle, Port Bloc, Boucau, St Jean de Luz, Bilbao, Santander 1 and 3. We exclude five tide gauges in the Bay of Biscay with too short or with too many gaps: Pointe Saint Gildas, Le Verdon, Pasajes, Santander 2 and Gijon 2. This step allows to complete mean-sea level records that display gaps and to compute the associated uncertainties.
- Second, we estimate vertical ground motions at each tide gauge either using a GNSS station (*Santamaría-Gómez et al.* 2012) or an estimate of the GIA effect (*Jevrejeva et al.* 2014). In the first case, the uncertainties are based on the analysis of the GNSS time series. In the second case, an uncertainty of $\pm$ 2mm/y is assigned, which is the standard deviation of the empirical distribution of the difference between vertical motion trends from GNSS records in the Sonel database and the GIA (*Wöppelmann and Marcos* 2006).
- Third, using the local vertical ground motions and past mean sea-level changes obtained at the two previous steps, we compute local geocentric mean sea-level changes and their uncertainties, assuming they are Gaussian.
- Finally, we use a weighted least square model to reconstruct a yearly time series of the regional geocentric mean sea-level changes curve.

Because the Bay of Biscay includes many high-quality tide gauge records and GNSS stations (e.g., Brest, Newlyn), our reconstructed curve compares well with other sea-level reconstructions based on tide gauge records, ocean models and altimetric measurements (*Meyssignac et al.* 2012), as well as to the records in Brest, which is the longest tide gauge in the region and where vertical motions are small (*Poitevin et al.* 2019).

A.2 Reconstruction of relative past sea-level changes in Gâvres

To transform the absolute mean-sea level reconstruction obtained above to values relative to the ground in Gâvres, we use an estimation of the local vertical land movement (VLM) in Gâvres based on the 3 nearest GPS stations provided by the SONEL network (*Santamaría-Gómez et al.* 2017). Table 4 shows the station information and VLM trend extracted from the SONEL platform. The 3 stations exhibit a slightly negative vertical land motion (subsidence). The mean of the trends (computed with the least mean square method) provides a vertical land movement of -0.33 ± 0.15 mm/y. The final relative mean sea level time series (MSL) is plotted in Figure 5.

Table 4 GPS station information and velocity of the vertical land motion, extracted from SONEL platform the 29th of October 2019, for the 3 nearest stations to Gâvres.

Name	Lat (°)	Lon (°)	Time period	Velocity (mm/y)
Kone	47.866	-3.902	11/2007 - 10/2019	-0.46 m $\pm$ 0.32
GROI	47.648	-3.508	10/2002 - 03/2015	-0.10 m $\pm$ 0.33
SARZ	47.524	-2.770	05/2007 - 10/2019	-0.36 m $\pm$ 0.20

B Quantile-Quantile corrections for the hydro-meteorological database

The figures below show the initial and corrected distribution of the surge, wave, and wind datasets used to build the hydro-meteorological database. These figures are plotted for the calibration periods (i.e. for the periods corresponding to the red areas in Figure 4a). For each dataset, this correction is then applied for the rest of the period (in white in Figure 4a).

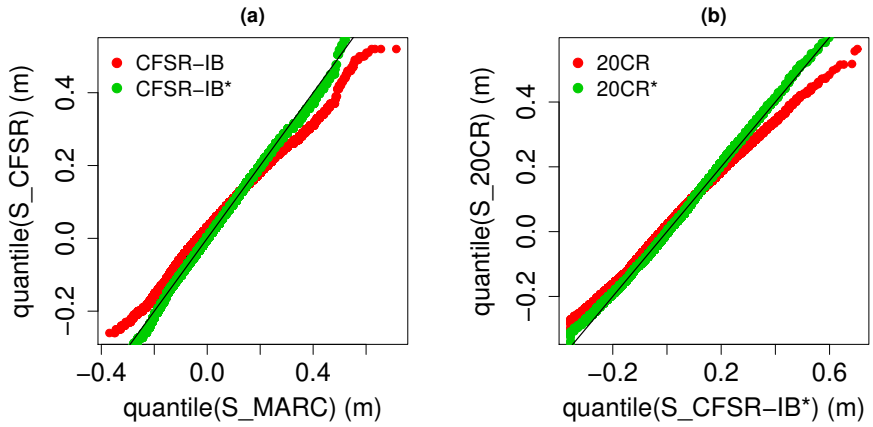

Fig. 15 Quantile-quantile corrections of surge data. QQ plots of the reference (MARC), data to correct and corrected data. (a) CFSR-IB data corrected with MARC data, (b) 20CR-IB data corrected with MARC data.

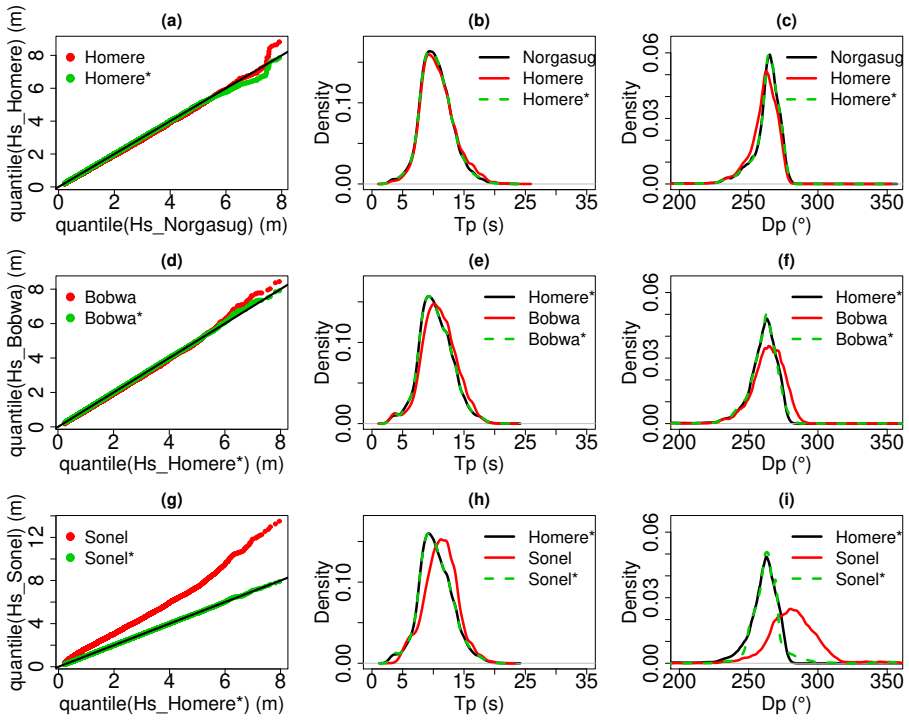

Fig. 16 Quantile-quantile corrections of wave data. QQ plots of wave height, probability density function (smoothed) of wave peak period and peak direction. (a,b,c) Homere data corrected with Norgasug data, (c,d,e) BOBWA data corrected with the corrected Norgasug data, (c,d,e) Sonel-waves data corrected with the corrected Norgasug data.

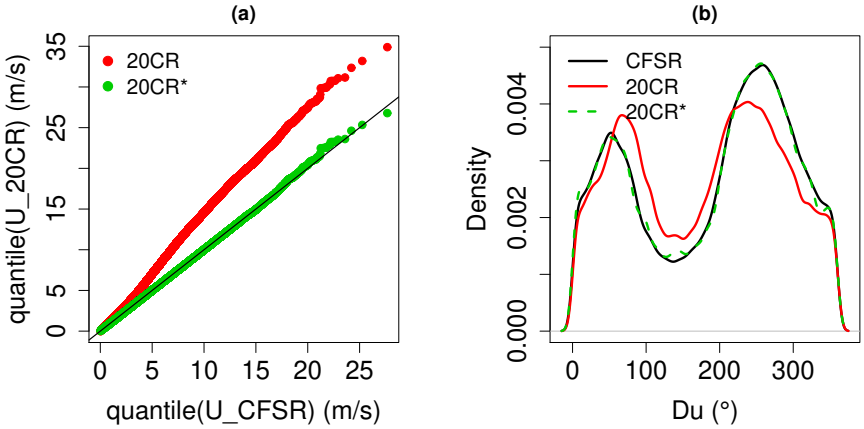

Fig. 17 Quantile-quantile corrections of the 20CR wind data using the CFSR wind data. QQ plots of wind speed (a) and probability density function (smoothed) of wind direction (b).

C Damage events and associated hydro-meteorological conditions

Table 5 shows an extract of the damage events, containing all the events, the dates, and the flood and confidence information. The corresponding hydro-meteorological conditions extracted from the HMD are given in Figure 18. The begin and end dates of (old) damage events are sometimes not very precise due to the lack of historical information. In these cases, the hydro-meteorological conditions selection method consists in selecting the highest tide during the period, as well as the high tide which is the closest to the highest wave height. This implies that for some events, two dataset of hydro-meteorological conditions can be selected (see e.g. the damage event n°40 for instance in the following table). When two dataset of hydro-meteorological conditions are associated to a flood event, we consider the most penalising conditions (based on flood simulations). Among the flood events, there is only one (Nd n°29) which corresponds to two hydro-meteorological scenarios. The analysis of the values suggests that the event occurs for the most penalising scenario, i.e. hydro-meteorological conditions dataset numbered Nhm=49. See Table 3 for the selected hydro-meteorological conditions of each flood event.

Table 5 Damage events, estimated flood (F, with the classification: 0 for no flood, 1 for moderate flood event, 2 for significant flood event) and confidence (C, with the classification: 1 for medium confidence, 2 for high confidence) indicators. Nd is the numbering in the damage events. F1 and C1 refer to the first version of the database. F2 and C2 refer to the second version, after the use of the numerical model.

Nd	Date(begin)	Date(end)	F1	C1	F2	C2
1	13/02/1900	15/02/1900	0	1	0	2
2	01/02/1904	02/02/1904	1	1	2	1
3	07/12/1911	09/12/1911	0	1	0	2
4	27/01/1922	29/01/1922	0	1	0	2
5	11/04/1922	11/04/1922	0	1	0	2
6	12/10/1922	20/10/1922	0	1	0	2
7	09/01/1924	09/01/1924	2	2	2	2
8	26/11/1924	27/11/1924	0	1	0	2
9	28/12/1924	29/12/1924	0	1	0	1
10	08/11/1927	09/11/1927	0	1	0	2
11	22/03/1928	23/03/1928	0	1	0	1
12	27/01/1936	27/01/1936	0	1	0	2
13	14/03/1937	14/03/1937	0	1	0	1
14	23/12/1945	23/12/1945	0	1	0	1
15	24/03/1947	24/03/1947	0	1	0	1
16	01/01/1948	28/02/1948	0	1	0	1
17	05/02/1950	06/02/1950	0	1	0	1
18	08/12/1954	09/12/1954	0	1	0	1
19	14/02/1957	15/02/1957	0	1	0	1
20	01/12/1959	01/12/1959	0	1	0	1
21	02/11/1963	03/11/1963	0	1	0	2
22	21/02/1966	22/02/1966	0	1	0	1
23	01/11/1967	04/11/1967	0	1	0	1
24	01/11/1972	31/12/1972	0	1	0	2
25	16/01/1974	11/02/1974	0	1	0	1
26	28/01/1975	29/01/1975	0	1	0	2
27	01/11/1975	30/11/1975	0	1	0	2
28	25/10/1976	25/10/1976	0	1	0	1
29	26/02/1978	26/02/1978	2	2	2	2
30	01/12/1978	31/12/1978	0	1	0	1
31	20/01/1980	20/01/1980	0	1	0	2
32	13/12/1981	13/12/1981	0	1	0	2
33	24/12/1981	24/12/1981	0	1	0	2
34	21/12/1983	21/12/1983	0	1	0	1
35	22/11/1984	23/11/1984	0	1	0	1
36	07/04/1985	08/04/1985	0	1	0	1
37	26/09/1999	26/09/1999	0	1	0	2
38	24/10/1999	24/10/1999	0	1	0	1
39	24/12/1999	29/12/1999	0	1	0	1
40	29/09/2000	29/09/2000	0	1	0	2
41	30/10/2000	30/10/2000	0	1	0	1
42	10/01/2001	10/01/2001	2	2	2	2
43	07/02/2001	07/02/2001	1	2	1	2
44	27/10/2004	27/10/2004	1	2	1	2
45	02/12/2005	02/12/2005	0	1	0	1
46	10/03/2008	10/03/2008	2	2	2	2
47	10/02/2009	10/02/2009	1	2	1	2
48	28/02/2010	28/02/2010	1	2	1	2

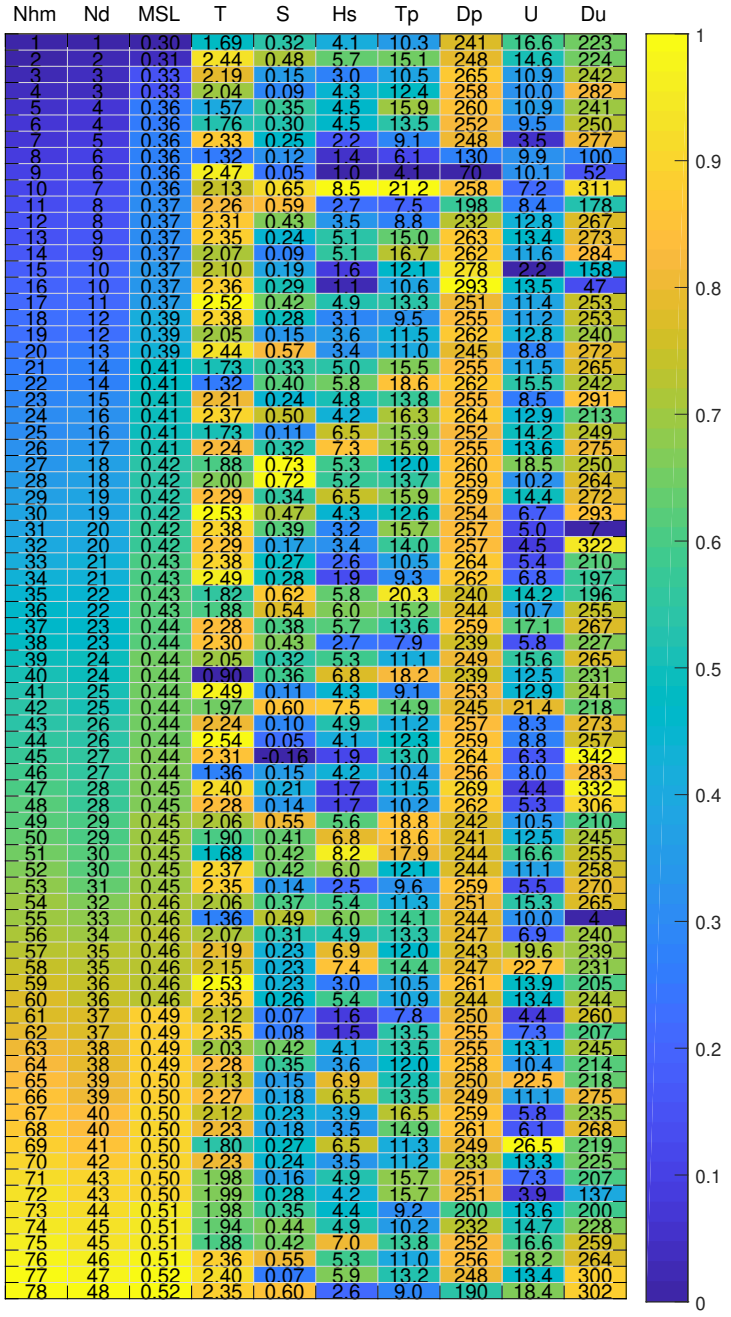

Fig. 18 Hydro-meteorological conditions extracted from the database for each damage events of table 5 with a rescaled colorbar. Nd and Nhm are the numbering in the damage events and hydro-meteorological events database, respectively. The other columns indicate the values of the following hydro-meteorological parameters: mean sea level (MSL, in meter referenced to IGN69 system), tide (T, in meter), atmospheric storm surge (S, in meter), significant wave height (H_s, in meter), wave peak period (T_p, in second), wave peak direction (D_p, in degree, nautical convention), wind speed (U, in meter per second), wind direction (D_u, in degree, nautical convention).

D Bivariate extreme value analysis

Bivariate extreme value analysis (bEVA) is performed focusing on the still water level relative to the mean sea-level ($\xi_{/MSL} = \xi - MSL$) and wave height (Hs).

The objective of bEVA is to extrapolate the joint probability density of the offshore sea condition variables to extreme values with appropriate consideration of the dependence structure. We follow a similar procedure as the one described by *Nicolae-Lerma et al.* (2018), which holds as follows:

- We use the 1900-2016 HMD to extract the values of wave height (Hs) and of skew surge (SS) at each high tide, using the reconstructed tide (T) and surge (S) time series;
- The marginals of Hs and SS are modelled by the combination of the empirical distribution, below a suitable high threshold u, with the Generalised Pareto distribution (GPD), above the selected threshold u (*Coles and Tawn* 1991) using the method of moments. The threshold value is selected by a combination of methods (visual inspection of quantile–quantile graphs, "mean residual life plots", "modified scale and shape parameters plots" ; see *Cales* 2001), which yield $u_{Hs} = 6.2$m and $u_S = 0.48$m. The marginal of $\xi_{/MSL}$ is estimated by combining the marginal of the skew surge (SS) with the empirical probability distribution of tides (T) by following the convolution approach of *Simon* (1994). This approach implicitly assumes that there is no interaction between tide and surge, an assumption which is justified on the study site of Gâvres after the study of *Idier et al.* (2012);
- The dependence structure of the variables $(\xi_{/MSL}; Hs)$ (with prior transformation into common standard Gumbel margins) is modelled by following the approach by *Heffernan and Tawn* (2004). This is based on a non-linear regression model that is fitted above a given threshold; hereby selected at 0.95 (expressed as a probability of non-exceedance) by using the diagnostic tools described in *Heffernan and Tawn* (2004);
- Once fitted, a Monte Carlo simulation procedure is used to randomly generate realizations of the variables $(\xi_{/MSL}; Hs)$. A total number of more than 6 millions of events are generated, which virtually represent a 100,000 year-period;
- Finally, the joint exceedance contour (*Hawkes et al.* 2002) is estimated, i.e. the contour (x, y) within the space $(\xi_{/MSL}; Hs)$ whereby the joint exceedance probability $Pr(\xi_{/MSL} > x, Hs > y)$ is constant (and equal to the probability associated to the return period of interest) at every point around the contour.